

Streamwise structures and density patterns in rapid granular Couette flow: a linear stability analysis

By MEHEBOOB ALAM

Engineering Mechanics Unit, Jawaharlal Nehru Center for Advanced Scientific Research,
Jakkur PO, Bangalore 560064, India
meheboob@jncasr.ac.in

(Received 25 January 2005 and in revised form 5 August 2005)

A three-dimensional linear stability analysis has been carried out to understand the origin of vortices and related density patterns in bounded uniform-shear flow of granular materials, using a kinetic-theory constitutive model. This flow is found to be unstable to pure spanwise stationary perturbations ($k_z \neq 0$, $k_x = 0$ and $\partial/\partial y(\cdot) = 0$, where k_i is the wavenumber for the i th direction) if the solid fraction is below some critical value $\nu < \nu_{3D}$. The growth rates of these spanwise instabilities are an order of magnitude larger than those of the two-dimensional ($k_z = 0$) streamwise-independent ($k_x = 0$) instabilities that occur if the solid fraction is above some critical value $\nu > \nu_{2D}$ ($> \nu_{3D}$). The spanwise instabilities give birth to new three-dimensional travelling wave instabilities at non-zero values of the streamwise wavenumber ($k_x \neq 0$) in dilute flows ($\nu < \nu_{3D}$). For moderate-to-large densities with $k_x \neq 0$, there are additional three-dimensional instability modes in the form of both stationary and travelling waves, whose origin is tied to the corresponding two-dimensional instabilities.

While the two-dimensional streamwise-independent modes lead to the formation of stationary streamwise vortices for moderately dense flows ($\nu > \nu_{2D}$), the pure spanwise modes are responsible for the origin of such vortices in the dilute limit ($\nu < \nu_{3D}$). For more general kinds of perturbations ($k_x \neq 0$ and $k_z \neq 0$), ‘modulated’ streamwise vortices are born which could be either stationary or travelling depending on control parameters. The rolling motion of vortices will lead to a major redistribution of the streamwise velocity and hence such vortices can act as potential progenitors for the mixing of particles. The effect of non-zero wall slip has been investigated, and it is shown that some dilute-flow instabilities can disappear with the inclusion of the wall slip. Even though the streamwise granular vortices have similarities to the well-known stationary Taylor–Couette vortices (which are ‘hydrodynamic’ in origin), their origin is, however, tied to ‘constitutive’ instabilities, and hence they belong to a different class.

1. Introduction

Rapid granular flows exhibit a rich phenomenology of particle clustering (Goldhirsch & Zanetti 1993; Luding & Herrmann 1999), segregation (Ottino & Khakhar 2000) and pattern formation (Umbanhower, Melo & Swinney 1996; Goldhirsch 2003). Some recent experiments on chute flows (the flow down an inclined plane) uncovered many interesting patterns in the form of roll waves, Kelvin–Helmholtz instability, fingering instability and streamwise vortices (Pouliquen, Delour & Savage 1997; Forterre & Pouliquen 2002; Goldfarb, Glasser & Shinbrot 2002).

Instability-induced patterns have been extensively studied in classical fluid mechanics for more than a century starting with the seminal works of Faraday, Rayleigh and Reynolds in the late nineteenth century. In this regard, the plane Couette flow has served as a prototype for such transition studies in Newtonian fluids. Following the classical approach of hydrodynamic stability, similar theoretical studies on the plane Couette flow of granular materials emerged during the end of last century (Mello, Diamond & Levine 1991; Savage 1992; Babić 1993; McNamara 1993; Schmid & Kytömaa 1994; Wang, Jackson & Sundaresan 1996; Tan & Goldhirsch 1997; Alam & Nott 1997, 1998; Nott *et al.* 1999) to explain particle clustering as an instability of the associated base flow. Most recently, Conway & Glasser (2004) have conducted large-scale molecular dynamics simulations of granular Couette flows to verify the emergence of various types of density patterns as predicted earlier by the linear stability analyses of Alam & Nott (1998).

Most of the previous stability studies on unbounded shear focused on two-dimensional flows (Savage 1992; Schmid & Kytömaa 1994; Wang *et al.* 1996; Tan & Goldhirsch 1997; Alam & Nott 1997, 1998), even though it is known that Squire's theorem does not hold for a granular fluid. Mello *et al.* (1991) considered the stability of a three-dimensional unbounded granular shear flow, allowing perturbations only in the 'mean' vorticity direction, and found that the flow can be unstable to such perturbations. Babić (1993) also studied the same problem by allowing a more general kind of time-dependent disturbance (known as Kelvin modes). He computed initial growth rates of instabilities and showed that the perturbations with large wavelengths initially grow exponentially, which might be responsible for particle clustering (provided that the time scales for instabilities are faster than that of the base flow). Wang *et al.* (1996) also briefly investigated the stability of unbounded shear flow to streamwise-independent ($k_x = 0$) modes. They showed that the flow is unstable to pure spanwise perturbations ($k_z \neq 0$, but $k_x = 0$ and $k_y = 0$) below a critical solid fraction. A review of all previous work on the unbounded shear flow was provided in Goddard & Alam (1999), along with some analytical results on its three-dimensional instability. It was shown that the unbounded shear flow remains stable to three-dimensional time-dependent Kelvin modes in the asymptotic limit, even though the flow could be unstable to pure spanwise perturbations for dilute flows ($\nu < \nu_{3D} \sim 0.1$, where ν is solid fraction). For pure transverse perturbations ($k_y \neq 0$, but $k_x = 0$ and $k_z = 0$), this flow remains unstable for $\nu > \nu_{2D}$ (~ 0.15). It was also shown that the most unstable mode in unbounded shear flow is of two-dimensional nature for $\nu > \nu_{2D}$, thereby satisfying the postulates of Squire's theorem for moderate-to-dense flows.

For the bounded Couette flow, however, all the stability analyses (Wang *et al.* 1996; Alam & Nott 1998; Nott *et al.* 1999; Alam *et al.* 2005; Alam 2005) investigated two-dimensional perturbations only. In contrast to its unbounded counterpart, these works clearly showed that there are additional two-dimensional instability modes, in the form of stationary and travelling waves, when the walls are imposed, even for the uniform shear flow. For a discussion on the relation between instabilities in unbounded and bounded shear flows, the reader is referred to Alam & Nott (1998).

Since Squire's theorem does not hold for granular flows, it is of interest to investigate the possibility of new three-dimensional instabilities in bounded Couette flow. Another important issue is the possible emergence of streamwise vortices and their modulated cousins in this flow. It is interesting to note that the streamwise vortices and their related streak patterns have recently been observed in experiments on granular chute flow and have also been predicted by the linear stability analysis of the associated

kinetic-theory continuum model (Forterre & Pouliquen 2002). Such vortical patterns have also been predicted to occur in Stokesian suspensions of colloidal particles (Carpen & Brady 2002), and observed in recent molecular dynamics simulations of dilute granular Couette flows (Conway & Glasser 2004).

From an altogether different viewpoint, we note that the streamwise vortices play an important role in transition to turbulence in shear flows of Newtonian fluids (Hamilton & Abernathy 1994; Schmid & Henningson 2001; Waleffe 2003). The understanding of the origin of such vortices in granular fluids could, thus, help in exploring the possibility of similar routes to turbulence in sheared granular flows. In this paper, we will try to answer whether the predicted streamwise vortices are likely to lead to turbulence or not. Owing to the lack of any existing systematic (and comprehensive) work on this, first we need to focus on uncovering different instabilities and related pattern formation mechanisms in granular shear flows.

This paper is organized as follows. In §2 we outline the continuum model and formulate the related three-dimensional linear stability problem. In §3 we present the stability results on bounded uniform shear flow, focusing on the formation of vortices, related density patterns and their characteristics in this flow. We have uncovered the analogues of the stationary vortices, along with asymmetric vortical patterns and other patterns. In §4.1 we discuss the possible effects of slip boundary conditions on the predicted instabilities. In §4.2 we discuss the origin of the streamwise-independent instabilities, and classify them according to constitutive/hydrodynamic instability. The present work is based on the Newtonian constitutive model of Lun *et al.* (1984); the implications of using a different constitutive model (e.g. Sela & Goldhirsch 1998; Garzo & Dufty 1999) are briefly discussed in §4.3. The conclusions are provided in §5, along with suggestions for future work.

2. Model

2.1. Constitutive model and non-dimensionalization

We consider a continuum-level description of granular materials, consisting of monodisperse particles of diameter \tilde{d} and material density $\tilde{\rho}_p$, bounded by two plane walls at $\tilde{y} = -\tilde{H}/2$ and $\tilde{y} = \tilde{H}/2$. The coefficient of restitution e (< 1) characterizes the inelastic nature of particle collisions. (In the following, the quantities with tildes are dimensional and those without are non-dimensional.) The upper wall moves with a velocity $\tilde{u}_w/2$ in the \tilde{x} -direction and the lower wall moves with the same velocity in the opposite direction. In the Cartesian framework, the \tilde{x} , \tilde{y} and \tilde{z} coordinates represent the streamwise, transverse (i.e. normal to the wall) and spanwise directions, respectively, with the corresponding velocity components being denoted by \tilde{u} , \tilde{v} and \tilde{w} , respectively. The mass density $\tilde{\rho} = \tilde{\rho}_p \nu$, with ν being the volume fraction of particles, and the velocity field $\tilde{\mathbf{u}} = (\tilde{u}, \tilde{v}, \tilde{w})^T$, are the standard hydrodynamic variables. In the rapid-shear regime (Kadanoff 1999; Goldhirsch 2003), the fluctuation kinetic energy (or the granular temperature)

$$\tilde{T} = \frac{1}{3} \langle (\tilde{\mathbf{c}}_i - \tilde{\mathbf{u}}) \cdot (\tilde{\mathbf{c}}_i - \tilde{\mathbf{u}}) \rangle = \frac{1}{3} \langle \tilde{\mathbf{C}}_i \cdot \tilde{\mathbf{C}}_i \rangle,$$

where $\tilde{\mathbf{c}}_i$ is the instantaneous velocity of the i th particle and $\tilde{\mathbf{C}}_i$ is its peculiar velocity, is also treated as a hydrodynamic variable. A separate balance equation for \tilde{T} (cf. the Reynolds stress equation in turbulence) is needed since the transport properties depend on the granular temperature. The dimensional form of these balance equations can be found elsewhere (Alam & Nott 1998).

The constitutive model for the stress tensor $\tilde{\Sigma}$ and the heat flux $\tilde{\mathbf{q}}$, with first-order corrections in inelasticity (and which is valid up to ‘linear’ gradients in the mean fields), reduces to the standard Newtonian model (Lun *et al.* 1984):

$$\tilde{\Sigma} = (\tilde{p} - \tilde{\zeta} \tilde{\nabla} \cdot \tilde{\mathbf{u}}) \mathbf{I} - 2\tilde{\mu} \tilde{\mathbf{S}}, \quad (2.1)$$

$$\tilde{\mathbf{q}} = -\tilde{\kappa} \tilde{\nabla} \tilde{T} - \tilde{\kappa}_h \tilde{\nabla} \nu, \quad (2.2)$$

where

$$\tilde{\mathbf{S}} = \frac{1}{2}(\tilde{\nabla} \tilde{\mathbf{u}} + \tilde{\nabla} \tilde{\mathbf{u}}^T) - \frac{1}{3}(\tilde{\nabla} \cdot \tilde{\mathbf{u}}) \mathbf{I}$$

is the deviatoric part of the rate of strain and \mathbf{I} is the identity tensor. Here \tilde{p} is the pressure; $\tilde{\mu}$ and $\tilde{\zeta}$ are the shear and bulk viscosities, respectively, of the granular fluid. For the constitutive model of heat flux, the proportionality constant for the standard Fourier term, $\tilde{\kappa}$, is the analogue of thermal conductivity. The additional transport coefficient, $\tilde{\kappa}_h$, that arises due to the gradients in particle volume fraction (and this can be thought of as the analogue of Soret effects in molecular fluids) is dubbed higher-order thermal conductivity since it is non-zero for a system of inelastic particles and vanishes identically for a perfectly elastic system. A simple functional form for the radial distribution function $\chi(\nu)$ is used in the present work,

$$\chi(\nu) = \frac{1}{1 - (\nu/\nu_{max})^{1/3}}, \quad (2.3)$$

that diverges in the random close packing limit ($\nu \rightarrow \nu_{max} \equiv 0.65$). The qualitative nature of our results remains unaltered even if we use the Carnahan–Starling expression for $\chi(\nu)$.

We use the wall-to-wall gap \tilde{H} as the length scale, the velocity difference between the walls \tilde{u}_w as the velocity scale and the inverse of the overall shear rate $\tilde{H}/\tilde{u}_w \equiv \tilde{\gamma}^{-1}$ as the time scale. With this scaling, the top wall of the Couette cell moves with a velocity 1/2 and the bottom wall with $-1/2$. The dimensionless governing equations and boundary conditions (Johnson & Jackson 1987) are written down in Appendix A. For the most of the results presented below, the usual no-slip and zero-heat-flux boundary conditions will be used, and the effects of wall slip on the stability results are considered in §4.1.

2.2. Base flow and linear stability equations

The base flow is steady ($\partial/\partial t = 0$) and fully developed ($\partial/\partial x = 0$). It can be verified that the continuity equation is identically satisfied, and the momentum and energy balance equations reduce to

$$\left. \begin{aligned} \frac{d}{dy} \left(\mu \frac{du}{dy} \right) &= 0, & \frac{dp}{dy} &= 0, \\ H^{-2} \frac{d}{dy} \left(\kappa \frac{dT}{dy} + \kappa_h \frac{d\nu}{dy} \right) + \mu \left(\frac{du}{dy} \right)^2 - \mathcal{D} &= 0, \end{aligned} \right\} \quad (2.4)$$

where $H = \tilde{H}/\tilde{d}$ is the Couette gap (in terms of particle diameter). The boundary conditions of no slip ($\mathbf{u}_s = 0$) and zero heat flux ($\mathbf{n} \cdot \mathbf{q} = 0$) admit an analytical solution to (2.4):

$$\nu(y) = \text{const.} = \nu_{av}, \quad u(y) = y, \quad T(y) = \frac{f_2(\nu, e)}{f_5(\nu, e)}, \quad (2.5)$$

for which the solid fraction and granular temperature are constants and the streamwise velocity varies linearly with y , i.e. the shear rate is uniform. (The dimensionless

functions f_1 – f_5 can be found in Alam & Nott (1998).) We will analyse the stability of this base flow.

To formulate the linear stability problem, the base flow $[v(y), u(y), 0, 0, T(y)]$ is perturbed by infinitesimal disturbances:

$$\left. \begin{aligned} v(x, y, z, t) &= v(y) + v'(x, y, z, t), \\ u(x, y, z, t) &= u(y) + u'(x, y, z, t), \\ v(x, y, z, t) &= v'(x, y, z, t), \\ w(x, y, z, t) &= w'(x, y, z, t), \\ T(x, y, z, t) &= T(y) + T'(x, y, z, t), \end{aligned} \right\} \quad (2.6)$$

where the primed quantities, which are much smaller in magnitude, denote three-dimensional perturbations. The time evolution of infinitesimal perturbations is studied by linearizing the equations of motion and the boundary conditions around the solution of (2.4). In operator form, the linear stability equations can be written compactly as

$$\frac{\partial X}{\partial t} = \mathcal{L}X, \quad \text{with } \mathcal{B}^\pm X = 0 \quad \text{at } y = \pm 1/2, \quad (2.7)$$

where

$$\left. \begin{aligned} \mathcal{L} &\equiv \mathcal{L}(\partial^j/\partial x^j, \partial^j/\partial y^j, \partial^j/\partial z^j, \dots), \\ \mathcal{B}^\pm &\equiv \mathcal{B}^\pm(\partial^j/\partial x^j, \partial^j/\partial y^j, \partial^j/\partial z^j, \dots), \end{aligned} \right\} \quad (2.8)$$

j is the order of the respective derivatives, and $X = (v', u', v', w', T')$ the vector of perturbation variables. The elements of the linear stability operator \mathcal{L} and the boundary operators \mathcal{B}^\pm are omitted for the sake of brevity.

It is straightforward to verify that the linear stability equations and the boundary conditions are invariant under translations in both x and z . This allows us to employ the standard Fourier method to decompose the perturbation variables into normal modes:

$$[v', u', v', w', T'](x, y, z, t) = [\hat{v}, \hat{u}, \hat{v}, \hat{w}, \hat{T}](y) e^{i(k_x x + k_z z) + \omega t}, \quad (2.9)$$

where the quantities with hats are complex amplitude functions of y ; k_x and k_z are the wavenumbers for the streamwise (x) and spanwise (z) directions, respectively. Here $\omega = \omega_r + i\omega_i$ is the complex frequency: ω_r determines the rate of growth/decay of perturbations and ω_i is the perturbation frequency. The stability/instability of the flow is determined by the sign of ω_r : for $\omega_r < 0$ the perturbations decay with time, signalling stability, and for $\omega_r > 0$ the perturbations grow with time, signalling instability; the flow is said to be neutrally stable for $\omega_r = 0$. The nature of the instability is determined by the value of ω_i : while $\omega_i = 0$ corresponds to a stationary wave, $\omega_i \neq 0$ corresponds to a travelling wave.

Substitution of the normal modes (2.9) into the stability equations (2.7) yields a differential eigenvalue problem:

$$\omega \hat{X} = \overline{\mathcal{L}} \hat{X}, \quad \text{with } \overline{\mathcal{B}}^\pm \hat{X} = 0 \quad \text{at } y = \pm 1/2, \quad (2.10)$$

where

$$\left. \begin{aligned} \overline{\mathcal{L}} &\equiv \mathcal{L}((ik_x)^j, d^j/dy^j, (ik_z)^j, \dots), \\ \overline{\mathcal{B}} &\equiv \mathcal{B}((ik_x)^j, d^j/dy^j, (ik_z)^j, \dots), \\ \hat{X} &\equiv (\hat{v}, \hat{u}, \hat{v}, \hat{w}, \hat{T}). \end{aligned} \right\} \quad (2.11)$$

Note that the linearized stability equations (2.10) remain invariant under the transformation

$$(x, y, z) \rightarrow (-x, -y, -z), \quad \omega \rightarrow \omega, \quad [\hat{v}, \hat{u}, \hat{v}, \hat{w}, \hat{T}] \rightarrow [\hat{v}, -\hat{u}, -\hat{v}, -\hat{w}, \hat{T}]. \quad (2.12)$$

This implies that there are conjugate pairs of modes with the same growth rate but having positive and negative phase velocities, which is a consequence of the centre-symmetry,

$$[v, u, T](y) = [v, -u, T](-y),$$

of the underlying base flow. In other words, the forward and backward propagating modes with the same growth rate coexist with each other.

2.3. Numerical method

To solve the eigenvalue problem (2.10), we have used a staggered-grid spectral (Chebyshev) collocation scheme to discretize the ordinary differential operators (Fornberg 1998; Alam & Nott 1998). The discretized stability equations, along with boundary conditions, form a generalized matrix-eigenvalue problem:

$$\mathbf{A}\Phi = \omega\mathbf{B}\Phi, \quad (2.13)$$

where \mathbf{A} and \mathbf{B} are square matrices of order $(5K+4)$, K is the degree of the Chebyshev polynomial, Φ the discrete analogue of the eigenfunction and ω the eigenvalue. Note that the matrix \mathbf{B} is singular since the boundary conditions do not contain time-derivatives. The standard row and column operations are performed to remove the singularity of \mathbf{B} , and the order of the matrices is thereby reduced to $(5K-4)$. The QR-algorithm of the MATLAB software is then used to calculate the eigenvalues of generalized eigenvalue problem (2.13).

Out of a total of $(5K-4)$ eigenvalues, the one with maximum growth rate for given stability parameters k_x and k_z ,

$$\omega_r^l = \max \omega_r,$$

is referred to as the *least stable* eigenvalue. The supremum of all least-stable modes over all k_x and k_z ,

$$\omega_r^d = \sup_{k_x, k_z} \omega_r^l,$$

is the *dominant* eigenvalue. Since the parameter space is very large (five control parameters: v_{av} , H , e , k_x and k_z), we have resorted to a detailed study of this three-dimensional stability problem at a few specific points in the (H, v_{av}) -plane, as shown by different symbols in figure 1. This figure shows four different types of instability regions for two-dimensional perturbations (Alam & Nott 1998).

3. Results: three-dimensional stability of bounded uniform shear flow

Here we present results for the three-dimensional instability of the uniform shear flow (2.5) for which the rigid ($\mathbf{u}_s = 0$, i.e. $u' = v' = w' = 0$) and the zero-heat-flux ($\mathbf{n} \cdot \mathbf{q} = 0$) boundary conditions hold. In the following, the *pure transverse* and *pure spanwise* modes refer to perturbations that have variations only in the transverse (y) and spanwise (z) directions, respectively. Most of the results are presented for a restitution coefficient of $e = 0.8$ (except in figures 12 and 15), and we comment on the robustness of our results in §4.3.

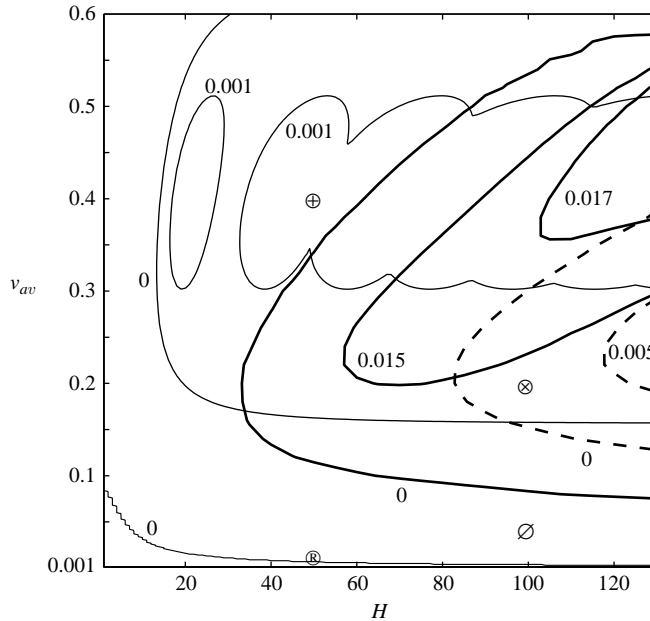


FIGURE 1. Stability diagram for granular shear flow subject to two-dimensional perturbations: $e = 0.8$ (adapted from Alam & Nott 1998). The symbols denote specific points to be discussed below.

3.1. Streamwise-independent instability ($k_x = 0$)

In this section, we focus on perturbations that do not vary along the streamwise direction (i.e. $k_x = 0$). For such streamwise-independent modes, the linear stability equations admit analytical solutions with the eigenfunctions being given in terms of exponentials in y :

$$[\hat{v}(y), \hat{u}(y), \hat{v}_1(y), \hat{w}_1(y), \hat{T}_1(y)] = [\hat{v}_1, \hat{u}_1, \hat{v}_1, \hat{w}_1, \hat{T}_1] e^{ik_n(y \pm 1/2)}. \quad (3.1)$$

Here $[\hat{v}_1, \hat{u}_1, \hat{v}_1, \hat{w}_1, \hat{T}_1]$ are the normalized amplitudes of perturbations, and $k_n = n\pi$ with n (a positive integer) being the mode number. In order to find the origin of streamwise vortices, we briefly recall the earlier results on the two-dimensional perturbations in §3.1.1.

3.1.1. Two-dimensional modes: transverse banding

For the two-dimensional ($k_z = 0$) transverse perturbations, it is known (Alam & Nott 1998) that the locus of neutral stability reduces to

$$H(v, e) = n\pi \sqrt{\frac{\mathcal{N}_1}{\mathcal{N}_2}} \sim (1 - e^2)^{-1/2}, \quad (3.2)$$

where

$$\mathcal{N}_1(v, e) = \frac{1}{f_5} \left[f_4 - f_{4h} f_1 \left(\frac{df_1}{dv} \right)^{-1} \right], \quad (3.3)$$

$$\mathcal{N}_2(v, e) = f_1 \left(\frac{df_1}{dv} \right)^{-1} \left[\frac{1}{f_5} \left(\frac{df_5}{dv} \right) + \frac{1}{f_2} \left(\frac{df_2}{dv} \right) \right] - 2. \quad (3.4)$$

It is clear from (3.2) that the $n = 1$ mode is the first to become unstable as H increases at a fixed v_{av} , and the onset of this instability represents the neutral stability contour

in the (H, ν_{av}) -plane as shown by the thin solid contour in figure 1. We observe that the flow is stable when the Couette gap is small; as H exceeds a critical value H_c , which is a function of ν_{av} and e , the flow becomes unstable. There is also a minimum value of solid fraction ($\nu_{av} \sim 0.156$), which is a weak function of e , below which the flow remains stable to two-dimensional perturbations (Alam & Nott 1998).

As discussed in previous works (Wang *et al.* 1996; Alam & Nott 1998), this pure transverse instability will lead to the segregation of particles, in the form of alternating bands of dilute and dense regions, along the transverse direction. Such transverse banding of particles is reminiscent of the shear-band formation in many complex fluids, and has been observed in molecular dynamics (MD) simulations of granular Couette flow (Tan 1995; Alam *et al.* 2005).

3.1.2. Pure spanwise modes: spanwise banding

For pure spanwise modes, $k_z \neq 0$, but $\partial/\partial y(\cdot) = 0$ and $\partial/\partial x(\cdot) = 0$. It can be verified that the dispersion relation can be factored into

$$\begin{aligned} & \left(\omega + \frac{\mu k_z^2}{\nu H^2} \right)^2 \left[\omega^3 + \left(\frac{2}{3\nu} (\mathcal{D}_T - u_y^2 \mu_T) + \frac{(2\mu + \lambda) k_z^2}{\nu H^2} + \frac{2\kappa k_z^2}{3\nu H^2} \right) \omega^2 \right. \\ & + \left(\frac{2\kappa(2\mu + \lambda) k_z^4}{3\nu^2 H^4} + \frac{2}{3\nu^2} (2\mu + \lambda) (\mathcal{D}_T - u_y^2 \mu_T) \frac{k_z^2}{H^2} + \frac{2pp_T k_z^2}{\nu^2 H^2} + \frac{p\nu k_z^2}{H^2} \right) \omega \\ & \left. + \frac{2}{3\nu} \left((p\nu\kappa - p_T\kappa_h) \frac{k_z^4}{H^4} + (p\nu(\mathcal{D}_T - u_y^2 \mu_T) - p_T(\mathcal{D}_v - u_y^2 \mu_v)) \frac{k_z^2}{H^2} \right) \right] = 0. \quad (3.5) \end{aligned}$$

The two real roots of (3.5), $\omega = -\mu k_z^2/\nu H^2$, are negative and hence stable. In fact, these two decaying modes correspond to the streamwise and transverse velocity fluctuations. This can be understood if we consider the linearized evolution equations for the streamwise and transverse velocity components:

$$\left. \begin{aligned} v \left[\frac{\partial u'}{\partial t} + u_y v' \right] &= \frac{\mu}{H^2} \frac{\partial^2 u'}{\partial z^2}, \\ v \frac{\partial v'}{\partial t} &= \frac{\mu}{H^2} \frac{\partial^2 v'}{\partial z^2}, \end{aligned} \right\} \quad (3.6)$$

which are decoupled from the other three equations for v' , w' and T' . It is straightforward to verify that the transverse velocity v' decays exponentially in time:

$$v'(t) = v_0 \exp(-t/\tau) \quad \text{with} \quad v_0 \equiv v'(t=0), \quad (3.7)$$

and the time constant is given by $\tau = \nu H^2/k_z^2 \mu$. The equation for the streamwise velocity u' is forced by v' , through its coupling with the mean shear u_y . The solution for u' is given by

$$u'(t) = (u_0 - v_0 u_y t) \exp(-t/\tau) \quad \text{with} \quad u_0 \equiv u'(t=0). \quad (3.8)$$

It is interesting to note that there could be a short-time growth for $u'(t)$, but in the asymptotic limit ($t \rightarrow \infty$) it decays with the same time constant τ as that of its transverse counterpart. The energy density for this mode ($E_u \sim u'^2$) would increase quadratically with time at small times, and the degree of transient energy growth would be large if the imposed shear rate were large. Clearly, the viscosity stabilizes both the streamwise and transverse velocity perturbations.

The other three stability equations for v' , w' and T' are coupled, leading to a cubic dispersion relation (3.5). It can be verified that this dispersion relation has one

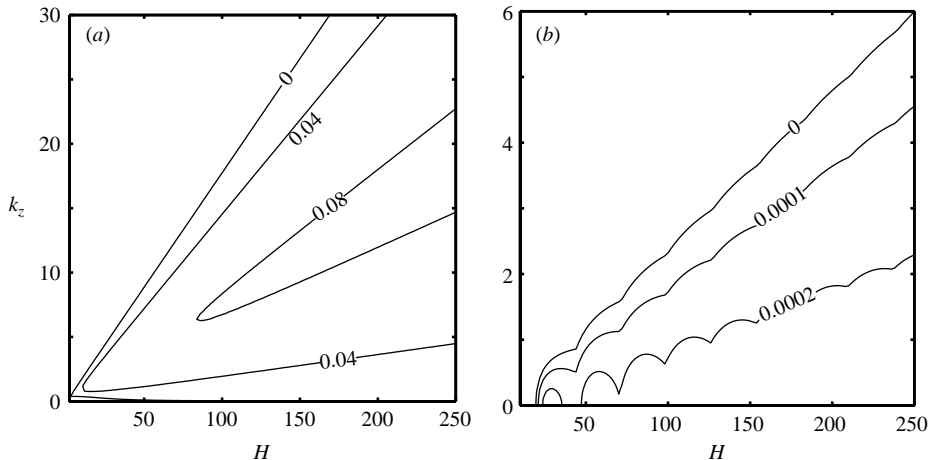


FIGURE 2. Stability maps for uniform shear flow in the (H, k_z) -plane for streamwise-independent modes ($k_x = 0$): (a) $v_{av} = 0.05$ and (b) 0.2 . The coefficient of restitution is $e = 0.8$. The outermost contour in each panel represents the contour of neutral stability.

real root and a complex-conjugate pair (Gayen & Alam 2005), and the instability is stationary. Hence, the locus of neutral stability can be simplified to

$$k_z^2 = H^2 \frac{\mathcal{N}_3(v, e)}{\mathcal{N}_1(v, e)} \sim (1 - e^2), \quad (3.9)$$

where

$$\mathcal{N}_3(v, e) = \left[f_1 \left(\frac{df_1}{dv} \right)^{-1} \left(\frac{1}{f_5} \left(\frac{df_5}{dv} \right) - \frac{1}{f_2} \left(\frac{df_2}{dv} \right) \right) - 1 \right]. \quad (3.10)$$

While $\mathcal{N}_1(v, e)$ remains positive for all values of v_{av} , $\mathcal{N}_3(v, e)$ can become negative beyond a moderate value of v_{av} (that refers to inadmissible solutions). The critical solid fraction, v_{3D} , above which this instability vanishes can be found by solving

$$\mathcal{N}_3(v, e) = 0.$$

This yields a value of $v_{3D} \approx 0.11$ which does not vary much with the restitution coefficient since $\mathcal{N}_3(v, e)$ is a weak function of e . It is clear from (3.9) that the range of spanwise wavenumbers, k_z , for which the flow is unstable, shrinks to zero in the elastic limit ($e \rightarrow 1$), i.e. the flow remains stable to pure spanwise perturbations for the case of perfectly elastic particles.

The pure spanwise instability leads to the segregation of particles, in the form of alternating bands of dense and dilute regions, along the mean-vorticity (spanwise) direction. It is interesting to point out that such spanwise banding of particles has recently been observed in large-scale MD simulations of granular Couette flow (Conway & Glasser 2004; Hopkins, Jenkins & Louge 1993), and is known to occur in many complex fluids (e.g. in micellar solutions; Fischer, Wheeler & Fuller 2002).

3.1.3. Onset of streamwise structures ($k_x = 0$ and $k_z \neq 0$)

Let us now focus on the streamwise-independent ($k_x = 0$) perturbations with non-zero values of the spanwise wavenumber ($k_z \neq 0$); this corresponds to perturbations that vary in both the transverse and spanwise directions.

Figure 2 shows two stability diagrams in the (H, k_z) -plane for $v_{av} = 0.05$ and 0.2 ; the restitution coefficient is set to $e = 0.8$. The contour of neutral stability is labelled

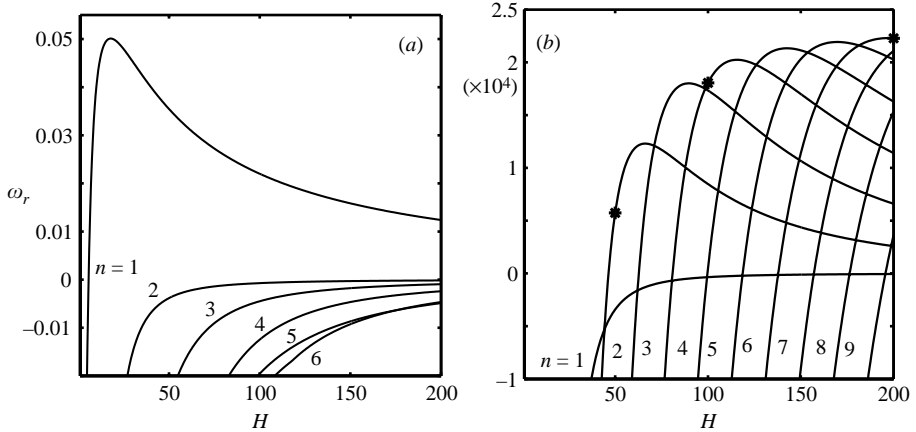


FIGURE 3. Variations of the growth rates of the first few modes with the Couette gap H : $e = 0.8$; $k_x = 0.0$; $k_z = 1$. (a) $v_{av} = 0.05$; (b) 0.2.

0, and the flow is unstable inside the neutral contour and stable outside. For dilute flows ($v_{av} = 0.05$, see panel *a*), the flow is unstable to a range of k_z , and this range of unstable k_z increases with increasing Couette gap. The origin of this instability can be traced back to the pure spanwise perturbations as discussed in the previous section. From the growth-rate contours in panel (a), we observe that the growth rate is negative at $k_z = 0$ and increases with increasing k_z , reaching a maximum at some value of k_z , and decreases thereafter. Increasing the mean solid fraction to $v_{av} = 0.1$ (not shown for brevity), the range of unstable k_z decreases, and this instability vanishes altogether for $v_{av} > v_{3D} \approx 0.11$. There is a window of solid fractions, $v_{3D} < v_{av} < v_{2D}$, for which the flow remains stable to streamwise-independent perturbations ($k_x = 0$). Beyond $v_{av} = v_{2D} \approx 0.16$, the pure transverse instability, as discussed in §3.1.1, takes over and the flow remains unstable to a range of k_z beyond a minimum Couette gap as seen in figure 2(b). For a given Couette gap, the growth rate of this instability is maximum at $k_z = 0$ and decreases with increasing k_z .

Figures 3(a) and 3(b) show the variations of the growth rate of the first few modes with the Couette gap for two densities $v_{av} = 0.05$ and 0.2, respectively – the spanwise wavenumber is set to $k_z = 1$, with other parameters as in figure 2. For dilute flows ($v_{av} = 0.05$, see panel *a*), the instability is due to the first mode, and all the higher-order modes remain stable. The growth rate of this mode increases with increasing H , reaches a maximum at some value of H , and decreases monotonically thereafter. At higher densities ($v_{av} = 0.2$, see panel *b*), the mode $n = 1$ remains stable for all H . For this parameter combination, the mode $n = 2$ becomes unstable first at some critical value of H and remains the most unstable mode for a range of H , and successive higher-order modes ($n = 3, 4, \dots$) take over as the most unstable mode after the mode $n = 2$ crosses the growth-rate curve of the mode $n = 3$ and so on. Such mode crossings (that represent degenerate eigenvalues) are responsible for resonance (Alam & Nott 1998) as well as the kinks observed on the growth rate curves in figure 2(b). Increasing the value of k_z to 3 makes the modes $n = 1, 2, 3$ and 4 stable for all Couette gaps, and the remaining modes with $n \geq 5$ can be unstable.

Let us now look at the eigenfunctions of the unstable modes. In the following, we have normalized the x - and z -coordinates by the streamwise wavelength (λ_x) and the spanwise wavelength (λ_z), respectively – hence each figure should be stretched by a factor of $2\pi/k_x$ or $2\pi/k_z$ in the streamwise or spanwise direction to ascertain the true

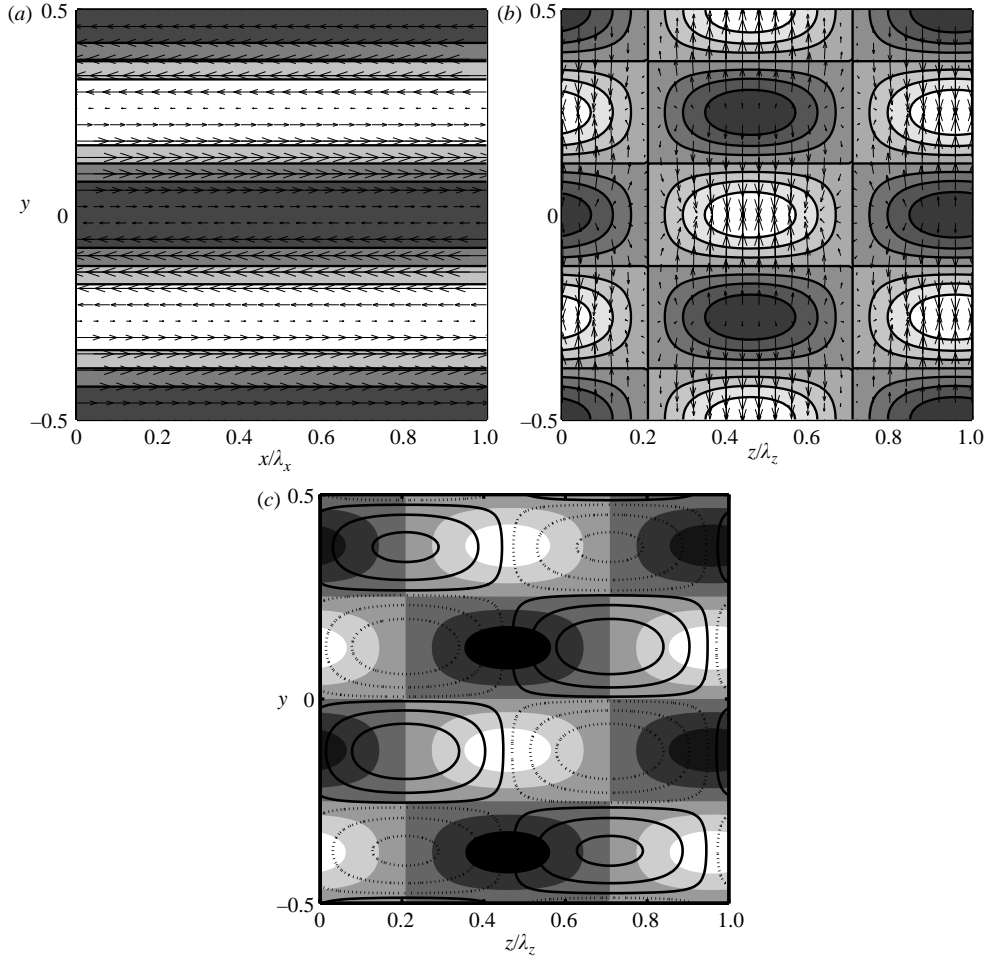


FIGURE 4. (a) Distributions of fluctuating density superimposed with the corresponding (u', v') velocity field in the (x, y) -plane (at $z=0$) for streamwise-independent modes ($k_x=0$). (b) Distributions of fluctuating density superimposed with the corresponding cross-flow (v', w') velocity field in the (y, z) -plane. (c) Shaded contours of the streamwise velocity $u'(y, z)$ in the (y, z) -plane, along with contours of streamwise vorticity $\Omega_x(y, z)$. Solid contours denote positive vorticity and dotted contours negative. Parameter values are $v_{av}=0.2$; $H=100$; $e=0.8$; $k_z=1.0$. On the grey scale, white denotes maximum (i.e. positive) and black minimum (i.e. negative).

aspect ratio of the underlying pattern. Figure 4(a) shows the disturbance pattern of solid fraction, overlaid with the corresponding fluctuating velocity-field (u', v') , in the (x, y) -plane for the most unstable mode in figure 3(b) at $H=100$ (i.e. the $n=4$ mode). On the grey scale, black represents minimum density and white maximum; the contours are drawn at equal intervals of solid fraction. There are two rows of particle-rich regions (white regions, called clusters) in figure 4(a), one located around middle of the upper-half-plane and the other around the middle of the lower-half-plane. The corresponding density pattern in the (y, z) -plane, along with the vector plot of the cross-flow velocity field (v', w') , is shown in figure 4(b). Looking at these velocity vectors, we find that the material accumulates in the denser vortex from the nearby dilute vortices.

The shaded contours of the streamwise velocity $u'(y, z)$ are shown in the (y, z) -plane in figure 4(c); as in the density plots, white represents positive (i.e. maximum) velocity and black negative (i.e. minimum). The contours of the streamwise vorticity Ω_x for the fluctuating motion,

$$\Omega_x = \frac{\partial w'}{\partial y} - \frac{\partial v'}{\partial z}, \quad (3.11)$$

are also superimposed. The solid contours denote positive Ω_x and the dotted contours negative Ω_x . This figure shows four counter-rotating streamwise vortices along the transverse direction and two per wavelength along the spanwise direction. Note that this vortex pattern does not change along the x -direction since $k_x = 0$. Clearly, the vortex rolls will lead to the redistribution of streamwise velocity, enhancing the mixing of particles.

We have noted in figure 3(b) that different modes take over as the most unstable mode as the Couette gap is varied (see, for example, the location of three stars on the growth-rate curves at three different Couette gaps). The overall disturbance patterns for the density, streamwise velocity and streamwise vorticity remain similar, except that the number of streamwise vortices increases with increasing H . For example, there are two vortices along the transverse direction at a Couette gap of $H = 50$ and seven at $H = 200$.

For dilute flows ($v_{av} = 0.05$, refer to figure 3a), the unstable disturbance pattern for solid fractions at $H = 100$, overlaid with the corresponding velocity field, is shown in figure 5(a) in the cross-stream plane. The parameter values are as in figure 3(a) with $k_z = 1$. The corresponding shaded contours of the streamwise velocity are shown in figure 5(b), along with the contours of positive (solid line) and negative (dashed line) streamwise vorticity Ω_x . We observe two counter-rotating vortices along the transverse direction, and this number does not change on increasing/decreasing the Couette gap. Note that the origin of these three-dimensional streamwise vortices is tied to the pure spanwise instability as discussed in §3.1.2. Increasing the spanwise wavenumber to $k_z = 10$ (see figures 5c and 5d) changes the structure of these vortices in that the vortical motion becomes more intense near the walls; this could be responsible for the birth of two additional ‘weaker’ bands of ‘excess’ streamwise velocity near the walls in figure 5(d). The overall structure of these patterns remains similar even if we change the Couette gap to $H = 50$ or 200. The reason for the appearance of two vortices in the transverse direction in figures 5(b) and 5(d) is that for three-dimensional spanwise perturbations, only the mode $n = 1$ is unstable and the higher-order modes remain stable for all Couette gaps.

It is interesting to note that similar streamwise rolls/vortices have recently been observed in three-dimensional molecular dynamics simulations of granular Couette flow (Conway & Glasser 2004). Their figure 11(e) shows three ‘modulated’ streamwise rolls parallel to the spanwise direction, and this corresponds to one density band along the transverse direction (located symmetrically around the mid-plane). Increasing the value of k_z by a factor of three (see their figure 11b), they found one streamwise roll in the spanwise direction. This is expected since increasing k_z is equivalent to decreasing the spanwise dimension of the Couette cell and hence it can accommodate fewer rolls. Note that the simulations of Conway & Glasser were restricted to dilute flows ($v_{av} = 0.05$), but with wall parameters that correspond to sink walls with non-zero wall slip. In contrast, all our results are valid for adiabatic walls with zero slip. Despite

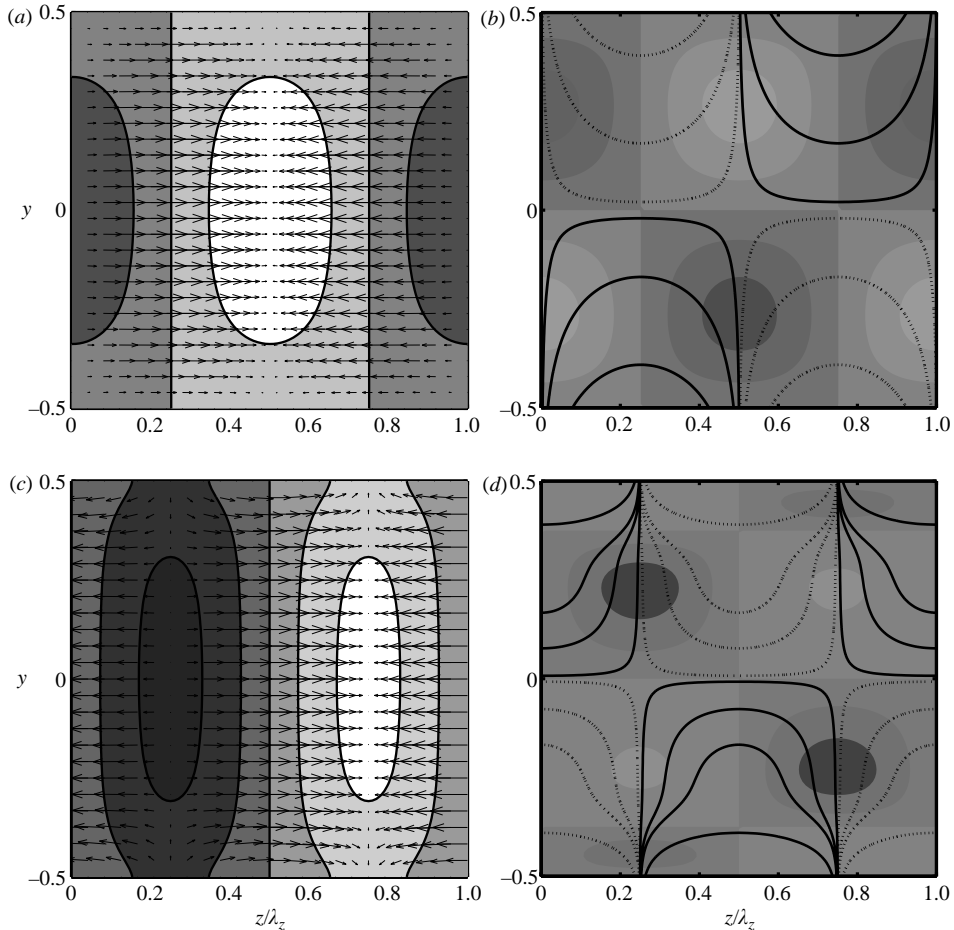


FIGURE 5. (a, c) Distributions of fluctuating density superimposed with the corresponding (v', w') velocity field in the (y, z) -plane for $k_x = 0$ at a low density $v_{av} = 0.05$. (b, d) Distributions of the streamwise velocity superimposed with the contours of Ω_x . Solid contours denote positive vorticity and dotted contours negative. The spanwise wavenumbers are (a, b) $k_z = 1$, (c, d) $k_z = 10$; other parameters as in figure 4.

different boundary conditions, we find qualitative agreement of our prediction of streamwise vortices with their observations.

The predicted streamwise vortices at low densities and the related density patterns are reminiscent of the well-known stationary Taylor–Couette vortices (Cole 1965) which have little variation along the azimuthal (i.e. streamwise, in plane Couette flow) direction. However, as we shall show in §4.2, the streamwise granular vortices belong to a separate class since they are non-hydrodynamic in origin.

3.2. General disturbances: modulated streamwise structures and density patterns

In this section, we consider instabilities that could arise from truly three-dimensional perturbations that vary in all three directions (i.e. $k_x \neq 0$, $k_z \neq 0$ and $\partial/\partial y(\cdot) \neq 0$), with a focus on uncovering ‘new’ three-dimensional instabilities and analysing their density and velocity patterns.

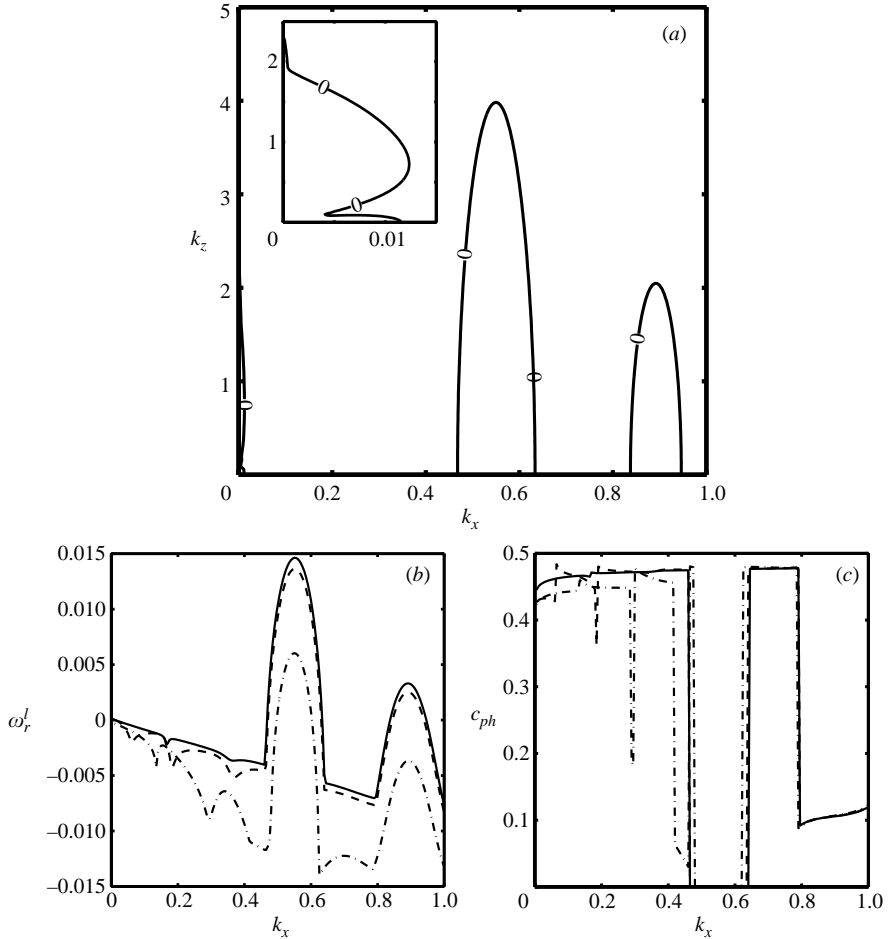


FIGURE 6. (a) Stability map in the (k_x, k_z) -plane for moderately dense flows at $v_{av} = 0.2$, $H/d = 100$ and $e = 0.8$. The inset shows the same at $k_x \sim 0$. (b, c) Variations of (b) growth rate and (c) phase velocity of the least stable mode with k_x for various values of k_z (solid lines, $k_z = 0$; dashed, $k_z = 1.0$; dash-dot, $k_z = 3.0$).

First we focus on the crossed-symbol, \otimes , in figure 1 at $v_{av} = 0.2$, $e = 0.8$ and $H = 100$. For these parameter values, figure 6(a) shows the stability map in the (k_x, k_z) -plane; the inset displays an expanded form of the stability map for very long streamwise wavenumbers $k_x \sim 0$. (The flow is unstable inside the neutral contour and stable outside.) Apart from the long-wave instabilities, there are two more unstable zones for moderate values of k_x . The variations of the growth rate, ω_r^i , of the least stable mode and its phase velocity, $c_{ph} = \omega_i/k_x$, with k_x are shown in figures 6(b) and 6(c), respectively, for three different values of the spanwise wavenumber k_z . It is clear from the phase-velocity curves that the unstable zone in figure 6(a), located around $k_x \sim 0.5$, is due to stationary waves and the one located around $k_x \sim 0.9$, is due to travelling waves. Looking at the variations of ω_r^i and c_{ph} for $k_z = 0$ in figures 6(b) and 6(c) (see also, figure 6 of Alam & Nott 1998), we conclude that *both these instabilities originate from the corresponding two-dimensional instabilities*. The effect of three-dimensionality (i.e. increasing k_z) is to decrease the growth rates of both the stationary and travelling instabilities. As in the two-dimensional case, the dominant

instability at $(H, v_{av}) = (100, 0.2)$ is due to the stationary waves. This conclusion holds at any other point in the (H, v_{av}) -plane that is located inside the neutral contour, denoted by the thick solid lines, in figure 1.

The (stationary) density-wave pattern along with the corresponding velocity vectors, for the dominant instability for $k_z = 1$ (see the dominant peak in figure 6*b*), is shown in figure 7(*a*) in the (x, y) -plane at $z = 0$. For this instability, $k_x = 0.55$ and hence figure 7(*a*) should be stretched by a factor of 11.4 in the x -direction to ascertain the true aspect of this pattern. The corresponding wave patterns in the (y, z) -plane at three different streamwise locations $x = 0$, $x = \lambda_x/2$ and $x = 3\lambda_x/4$ are shown in figures 7(*b*), 7(*c*) and 7(*d*), respectively. For all panels, the white denotes a positive quantity, and the black a negative. It is observed in figure 7(*a*) that there are four rows of clusters in the y -direction, in contrast to the corresponding two-dimensional pattern at $k_z = 0$ (not shown here, but see figure 8*a* of Alam & Nott 1998). Essentially, the cluster around the mid-plane for the two-dimensional case splits into two smaller clusters when the spanwise perturbations are allowed. We observe intense vortical motions around each cluster in figures 7(*b*), 7(*c*) and 7(*d*). The shaded contours of the streamwise velocity, $u'(y, z)$, at $x = 0$ are shown in figure 7(*e*), and those of the streamwise vorticity, Ω_x , in figure 7(*f*). Note that the streamwise vortices are modulated in shape (a consequence of the non-zero streamwise wavenumber), and are aligned at some angle with the streamwise direction. There is a strong vortex around the mid-plane and two relatively weaker vortices near the walls. The central vortex appears to be responsible for the splitting of the cluster (located around the mid-plane) as mentioned earlier. Comparing figures 7(*e*) and 7(*f*), we find that the streamwise vortices help to redistribute the streamwise velocity in the flow.

The travelling analogues of the stationary patterns as depicted in figures 7(*a*), 7(*b*), 7(*e*) and 7(*f*) are shown in figures 8(*a*), 8(*b*), 8(*c*) and 8(*d*), respectively. (This corresponds to the second peak on the growth-rate curve in figure 6*b* with $k_z = 1.0$). This is a backward travelling wave, and the related forward travelling pattern can be ascertained via the standard Euclidean group E_1 of transformation. The streamwise wavenumber for this instability is $k_x \approx 0.9$ and the phase velocity is $c_{ph} = -0.1$. Compared to its two-dimensional counterpart (see figure 8*b* of Alam & Nott), the elongated cluster around the mid-plane splits into two clusters of unequal size, and this splitting of clusters is due to the presence of the streamwise vortices below the mid-plane. The overall structural features of these density patterns and the associated vortical motions look similar to those of the dominant stationary instability in figure 7 since both have the same parental origin (Alam & Nott 1998).

Next we focus on the symbol \oplus in figure 1 for which $v_{av} = 0.4$, $H = 50$ and $e = 0.8$. Recall that for these parameter values, the dominant instability for two-dimensional perturbations is due to the pure transverse modes. The stability map in the (k_x, k_z) -plane, for three-dimensional perturbations at \oplus , is shown in figure 9(*a*). We observe that there are two instability lobes – one for small k_z (~ 0) and the other for moderate values of k_z . (Note that this stability map is similar to that for the long-wave modes at $v_{av} = 0.2$ and $H = 100$ as in the inset of figure 6*a*.) The variations of ω_r' and c_{ph} with k_z for three different values of k_x are shown in figures 9(*b*) and 9(*c*), respectively. Figure 10(*c*) suggests that these instabilities are travelling in nature. We observe in figure 9(*b*) that the most unstable mode for $k_x = 0.01$ occurs at $k_z \approx 0.2$ and hence it is a three-dimensional instability; increasing the value of k_x , however, shifts the most unstable mode to $k_z = 0$, i.e. a two-dimensional instability. Thus, there is a small window of streamwise wavenumbers ($k_x \sim 0$) for which the most unstable instability is due to a three-dimensional perturbation. We have checked that this observation

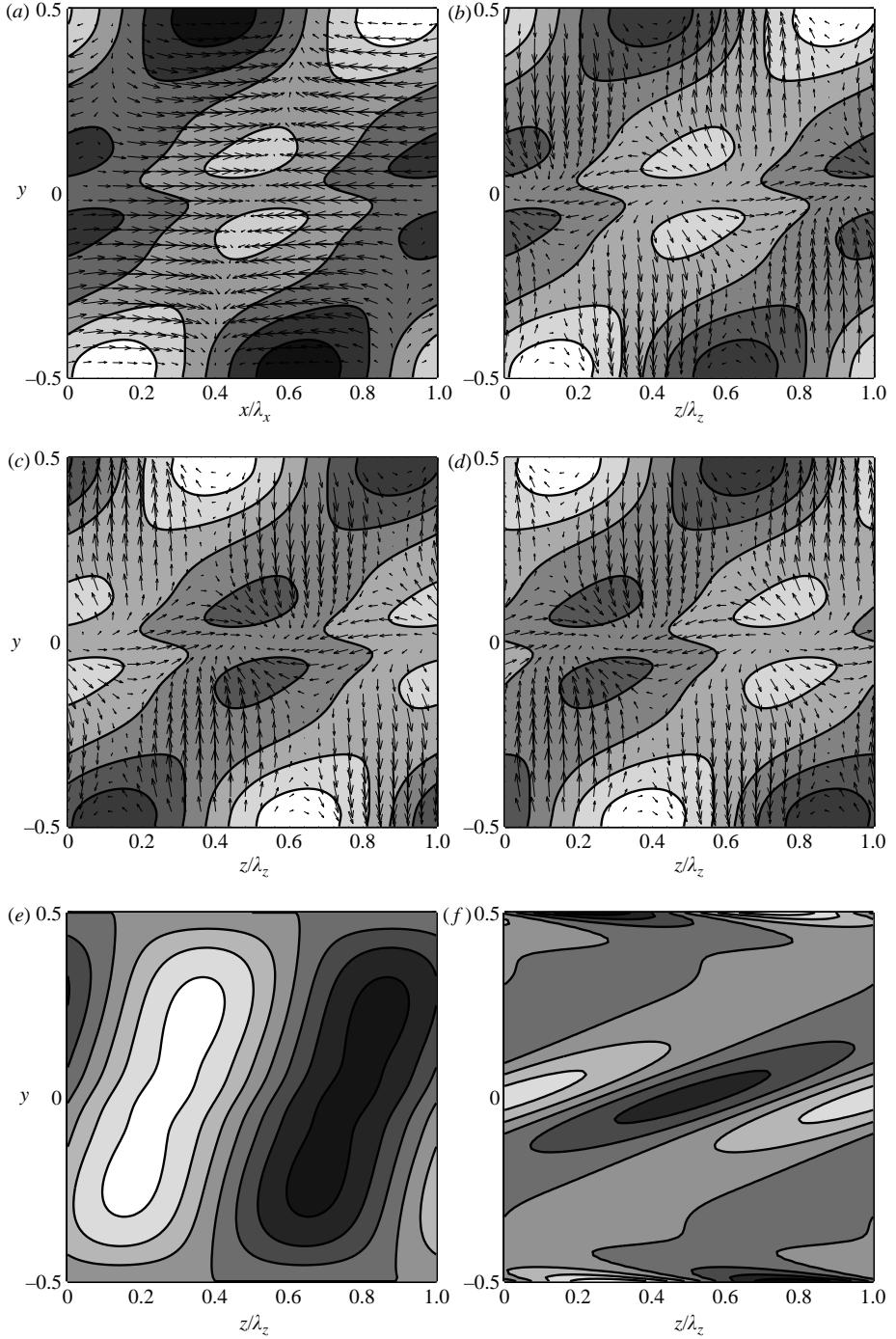


FIGURE 7. (a) Distributions of fluctuating density superimposed with the corresponding (u, v) velocity field in the (x, y) -plane at $z=0$. (b–d) Same as in (a) but in the (y, z) -plane at different streamwise locations: (b) $x=0$, (c) $x=\lambda_x/2$ and (d) $x=3\lambda_x/4$. Shaded contours of (e) streamwise velocity $u'(y, z)$ and (f) the streamwise vorticity Ω_x in the (y, z) -plane at $x=0$. The wavenumbers are $k_x=0.55$ and $k_z=1.0$, with other parameters as in figure 6. On the grey scale, white denotes maximum (i.e. positive) and black minimum (i.e. negative).

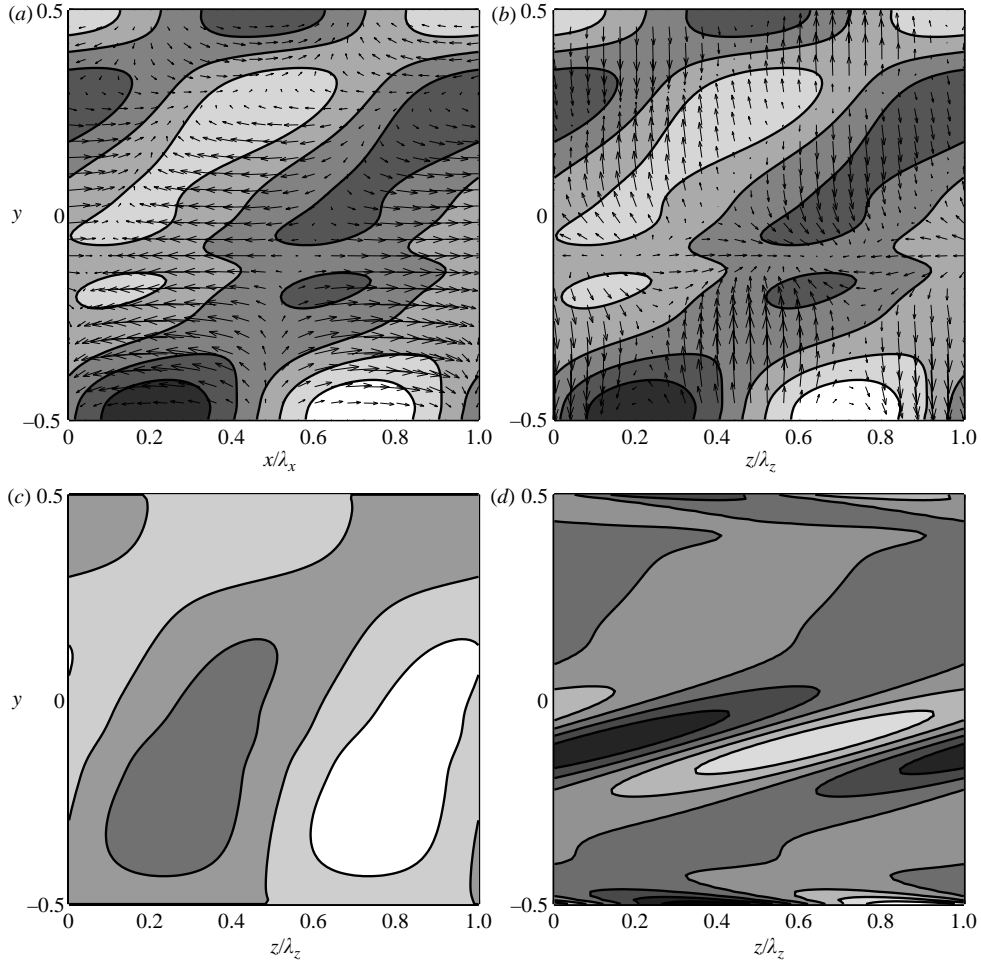


FIGURE 8. (a) Forward travelling wave pattern for the fluctuating density field superimposed with the corresponding velocity vectors in the (x, y) -plane at $z=0$. (b) The same as in (a) but in the (y, z) -plane at $x=0$. (c) Shaded contours of the streamwise velocity in the (y, z) -plane at $x=0$. (d) The same as in (c) but for the streamwise vorticity. The streamwise wavenumber is $k_x = 0.89$, with other parameters as in figure 7.

holds at any other point in the (H, v_{av}) -plane that is located between the neutral stability contour for the pure transverse modes (denoted by the thin solid lines in figure 1) and the neutral contour for the dominant stationary modes (denoted by the thick solid lines in figure 1).

Focusing on the symbol \odot in figure 1 for which $v_{av} = 0.05$, $H = 100$ and $e = 0.8$, we note that the flow is stable to two-dimensional perturbations. The stability map in the (k_x, k_z) -plane, for three-dimensional perturbations at \odot , is shown in figure 10(a). The variations of ω_r^l and c_{ph} with k_x for three different spanwise wavenumbers are shown in figures 10(b) and 10(c), respectively. We observe in figure 10(a) that there are two instability lobes – the slender lobe near $k_x \sim 0$ represents stationary waves and the larger lobe at large k_x represents travelling waves. This origin of the stationary instabilities is traced back to the pure spanwise instability as discussed in §3.1.2. Analysing the modal structure of the first few modes with k_x (not shown for

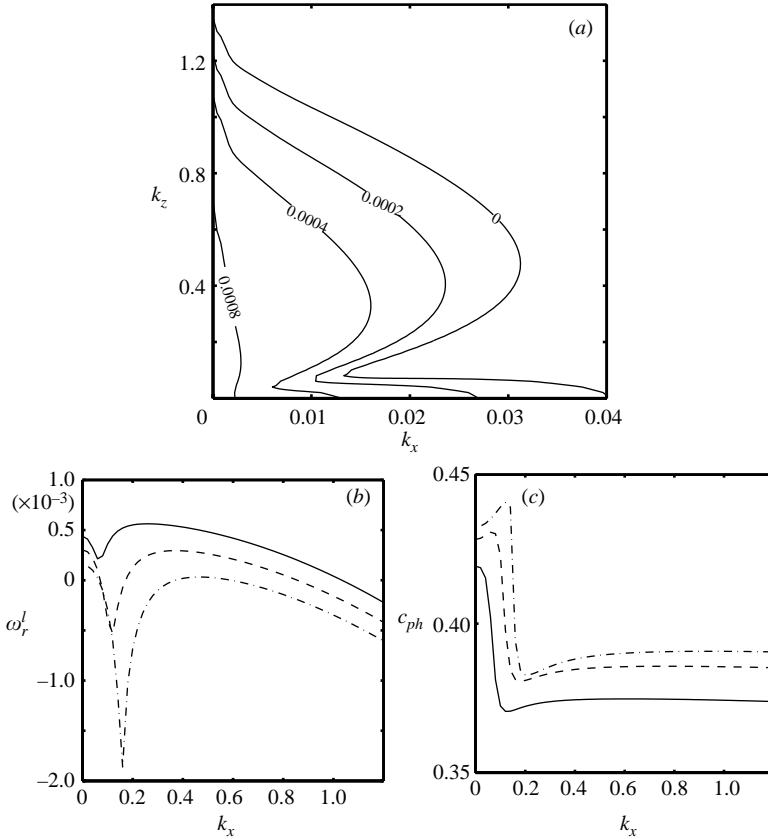


FIGURE 9. (a) Stability map in the (k_x, k_z) -plane at $v_{av}=0.4$, $H=50$ and $e=0.8$. (b, c) Variations of (b) growth rate and (c) phase velocity of the least stable mode with k_z for various values of k_x (solid lines, $k_x=0.01$, dashed, $k_x=0.02$; dash-dot, $k_x=0.03$).

brevity), we have found that these stationary instabilities at small k_x give birth to ‘new’ travelling instabilities at large k_x . The dominant instability at \odot still comes from the pure spanwise modes, but we have uncovered new three-dimensional travelling instabilities of comparable growth rates with $k_x = O(1)$.

The density distribution for a typical travelling instability pattern in the (x, y) -plane, at \odot with $k_x=1$ and $k_z=10$, is shown in figure 11(a) at $z=0$. This is a backward travelling wave, with the phase velocity $c_{ph} \approx -0.42$. The corresponding travelling pattern in the (y, z) -plane at $x=0$ is shown in figure 11(b). It is observed that the clusters are concentrated near the bottom wall along with large-scale vortical motions. There is hardly any fluctuating motion in the upper-half of the Couette cell. This is in contrast to the travelling wave patterns at moderate densities in figure 8 where we observed clustering and intense vortical motion over the whole Couette-cell. The nonlinear saturation of the instabilities in figure 10 will lead to asymmetric travelling density patterns, with the asymmetry being in the transverse direction.

Considering the stationary instabilities in figure 10 at very small values of k_x (~ 0.01), we have found (not shown for brevity) that the density patterns and the associated vortical motions remain similar to those in figure 5 (for $k_x=0$), with the only difference being that the density bands are now inclined to the streamwise direction.

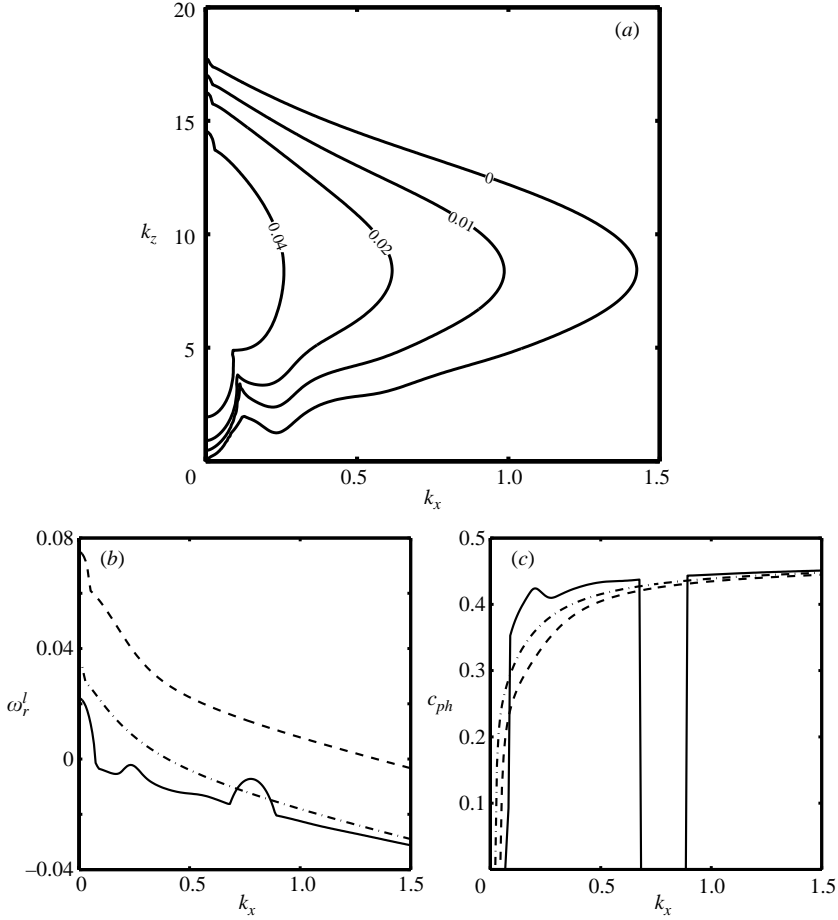


FIGURE 10. (a) Stability map in the (k_x, k_z) -plane for dilute flows at $v_{av} = 0.05$, $H = 100$ and $e = 0.8$. (b, c) Variations of (b) growth rate and (c) phase velocity of the least stable mode with k_x for various values of k_z (solid, $k_z = 1.0$; dashed, $k_z = 10.0$; dash-dot, $k_z = 15.0$).

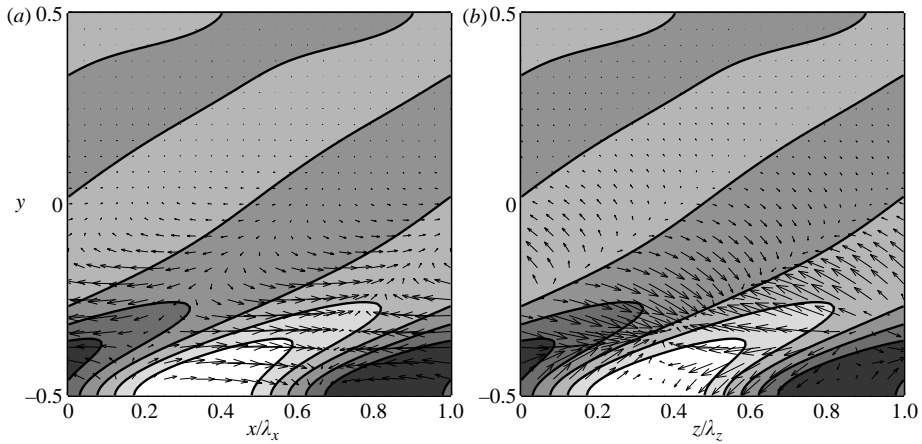


FIGURE 11. (a) Distributions of fluctuating density superimposed with the corresponding (u, v) velocity field in the (x, y) -plane at $z = 0$. (b) Distributions of fluctuating density superimposed with the corresponding (v, w) velocity-field in the (z, y) -plane at $x = 0$. The wavenumbers are $k_z = 10$ and $k_x = 1.0$, with other parameters as in figure 10.

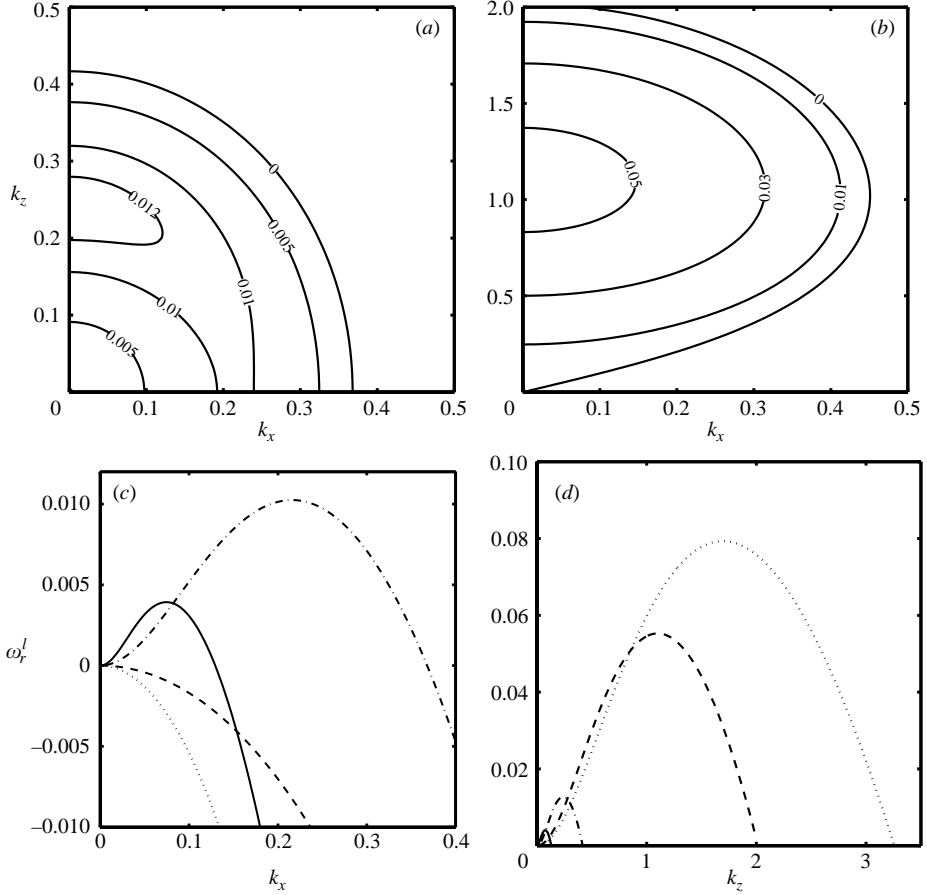


FIGURE 12. Stability maps in the (k_x, k_z) -plane for very dilute flows at $v_{av}=0.01$ and $H=50$ (refer to the circled-R symbol in figure 1): (a) $e=0.99$; (b) $e=0.8$. (c, d) Variations of growth rate with k_x or k_z : (c) $k_z=0$; (d) $k_x=0$ (dotted lines, $e=0.5$; dashed, $e=0.8$; dash-dot, $e=0.99$; solid, $e=0.999$).

Finally, we focus on the ‘circled-R’-symbol in figure 1 for which $v_{av}=0.01$ and $H=50$. For this parameter combination, the stability maps in the (k_x, k_z) -plane are shown in figures 12(a) and 12(b) for two restitution coefficients $e=0.99$ and 0.8 , respectively. We have checked that this instability corresponds to a stationary wave. It is observed that the instability zone increases in size with increasing dissipation levels. For the nearly elastic system (panel a) there is a range of k_x for two-dimensional perturbations ($k_z=0$) for which the flow is unstable; decreasing the restitution coefficient to $e=0.8$ (see panel b) makes the two-dimensional perturbations stable for all k_x . This is in contrast to other two-dimensional instabilities (as discussed above) which become stronger with increasing dissipation levels. This interesting dichotomy was noted by Alam & Nott (1998) as displayed in figure 12(c) where we have plotted the variations of ω_r^l with k_x for $k_z=0$ for four different restitution coefficients. Clearly, the growth rate of the two-dimensional dominant mode is maximum at some value of e and this instability degenerates into a neutral mode in both the perfectly elastic and dissipative limits. In fact, this is a three-dimensional instability that survives in the two-dimensional limit. This can be verified from figure 12(d) which shows the

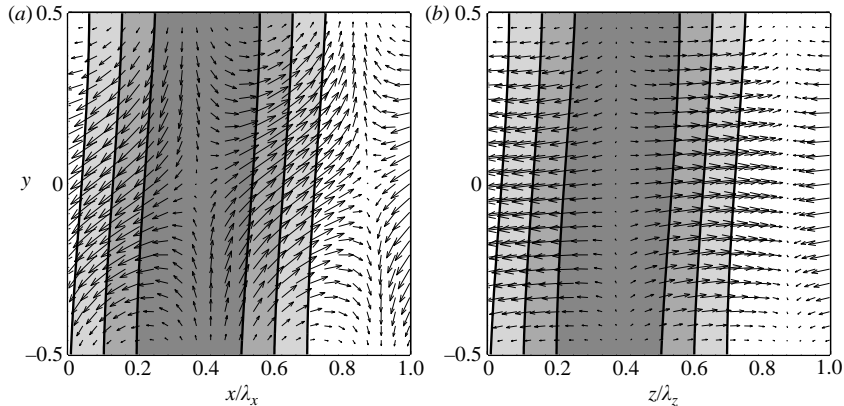


FIGURE 13. (a) Distributions of fluctuating density superimposed with the corresponding (u', v') velocity field in the (x, y) -plane at $z=0$. (b) Distributions of fluctuating density superimposed with the corresponding (v', w') velocity field in the (z, y) -plane at $x=0$: $v_{av}=0.01$, $H=50$, $e=0.8$, $k_z=1$; $k_x=0.1$.

variations of ω_r^l with k_z for three-dimensional perturbations with $k_x=0$. We observe that the range of unstable k_z and the maximum growth rate decrease in the elastic limit $e \rightarrow 1$.

Figure 13(a) shows the density distribution, overlaid with the corresponding velocity field, in the (x, y) -plane at $z=0$ for the stationary instability at $(v_{av}, H) = (0.01, 50)$ with $k_x=0.1$ and $k_z=1.0$. The corresponding pattern in the (y, z) -plane at $x=0$ is displayed in figure 13(b). (The cross-flow patterns at other streamwise locations look similar.) We observe a distinct pattern of vertical banding, i.e. the flow will degenerate into columnar structures along the transverse direction. Note that the vortical motion appears to be more intense in the (x, y) -plane than in the cross-flow plane.

4. Discussion

4.1. Effects of boundary conditions

Previous works on the stability of plane Couette flow to two-dimensional perturbations have established (Alam & Nott 1998) that the qualitative nature of the stability results does not change even if we impose wall-slip and non-zero heat-flux boundary conditions as long as the base flow remains similar to that of the uniform shear flow. Only the growth rates differ if the walls act as sources/sinks of the granular energy. For example, the growth rates of the dominant stationary and travelling instabilities (refer to figure 1) will increase/decrease if the walls are made energy sources/sinks, respectively.

We have verified that the above conclusions on two-dimensional instabilities also hold for their three-dimensional counterparts – the details of these results are omitted for the sake of brevity. However, the three-dimensional instabilities in the dilute regime (see figure 12) are affected by the wall slip in some significant way as we demonstrate below.

4.1.1. Effects of wall slip

In order to isolate the effects of wall slip on the stability characteristics of the uniform shear flow, we consider a uniform shear solution to (2.4) with

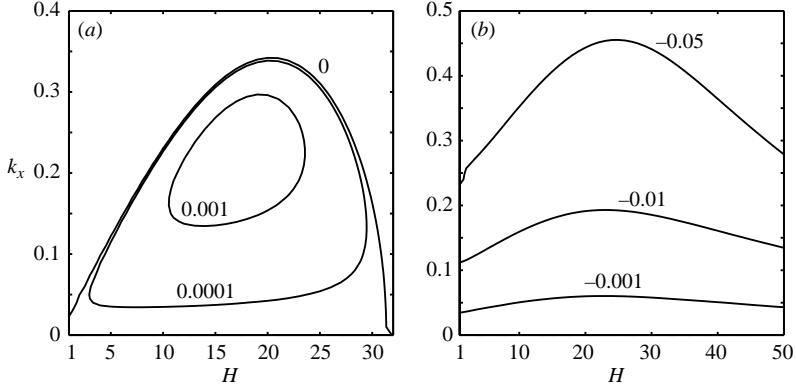


FIGURE 14. Effect of slip on the stability map in the (H, k_x) -plane at $(v_{av}, e) = (0.01, 0.8)$: (a) uniform-shear case; (b) uniform-shear case with slip.

non-zero slip:

$$\left. \begin{aligned} v(y) &= \text{constant}, \\ u(y) &= (1 - 2|u_s|)y, \\ T(y) &= \frac{f_2}{f_5}(1 - 2|u_s|)^2. \end{aligned} \right\} \quad (4.1)$$

Note that this solution arises when the production term balances the dissipation term in (A 8), leading to an adiabatic boundary condition on temperature. Here the slip velocity satisfies the relation

$$|u_s| = \frac{1}{(2 + \phi H f_7)}. \quad (4.2)$$

We refer to (4.1) as the uniform-shear case with slip which is valid for a set of wall-parameter combinations that is fixed by the following relation:

$$\phi(1 - e_w^2) = \frac{2f_5}{3f_2f_7^2}. \quad (4.3)$$

Here $e_w (\neq 1)$ is the restitution coefficient for particle–wall collisions, and ϕ is the specular coefficient. If we specify the mean solid fraction, v_{av} , and the material parameter, e , the right-hand side of (4.3) is known and hence e_w can be found as a function of ϕ . Thus, (4.1) provides an ideal base state to judge the effect of slip on stability by comparing its results with the uniform-shear case.

Figures 14(a) and 14(b) show the contours of ω_r^l in the (H, k_x) -plane for the cases of uniform shear (2.5) and uniform shear with slip (4.1), respectively. Parameter values are set to $v_{av} = 0.01$ and $e = 0.8$. Comparing these two figures, we find that the presence of slip makes the flow stable for the whole range of H . For $e = 0.8$, we have verified that the dilute flow instabilities are absent at other values of v_{av} , making the flow (4.1) stable to these instabilities in the (H, v_{av}) -plane. Thus, in a stability map such as in figure 1, the unstable zone in the lower left-hand corner is absent altogether for the uniform-shear case with slip.

To ascertain the effect of slip on slightly inelastic particles, we show the stability map in figure 15(a) in the (H, k_x) -plane for $e = 0.99$, with the mean density as in figure 14. The solid lines denote the contours of ω_r^l for the uniform-shear flow with slip (4.1), while the dashed line denotes the neutral contour for the no-slip case (2.5). It is observed that the effect of slip is simply to diminish the ranges of H and k_x for which the flow is unstable. It is interesting to note that the instabilities in the non-continuum

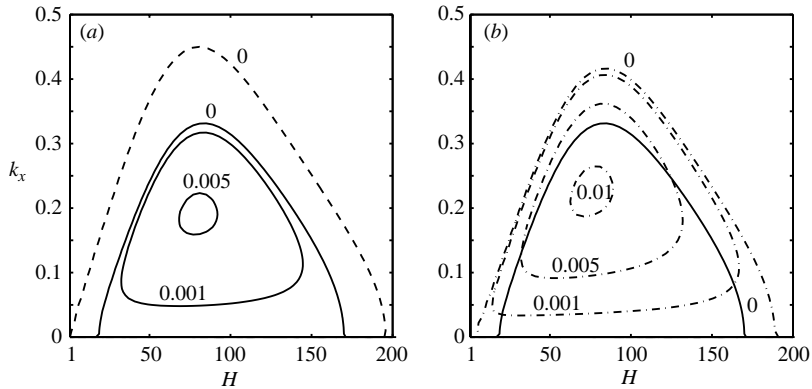


FIGURE 15. Stability maps in the (H, k_x) -plane at $v_{av} = 0.01$ and $e = 0.99$. (a) The solid lines denote the contours of ω_r^l for the uniform-shear case with slip, while the dashed line denotes the neutral contour for the uniform-shear case. (b) The dot-dash lines denote the contours of ω_r^l for source walls ($e = 0.99$ and $e_w = 1.0$), while the solid line denotes the neutral contour for the case of uniform-shear with slip.

limit ($H \rightarrow 0$) now disappear when the slip is incorporated. Our computations show that typical growth rates for (4.1) at any point inside the unstable zone in figure 15(a) are lower by an order of magnitude in comparison with the no-slip base state.

Lastly, figure 15(b) shows the contours of ω_r^l in the (H, k_x) -plane for the case of source walls ($e = 0.99$ and $e_w = 1.0$) at $v_{av} = 0.01$, denoted by the dot-dash lines. The neutral contour for the uniform-shear case with slip is also superimposed as a solid line. Comparing the two neutral contours, we find that the range of unstable H and k_x increases when the walls act as sources of granular energy, and the associated growth rates also increase marginally.

The above results indicate that the effect of slip is to diminish the dilute flow instability in that the ranges of unstable H , k_x and k_z , and the instability growth rate decrease with the inclusion of slip for slightly inelastic particles. At $e = 0.8$, these instabilities are completely suppressed by the wall slip.

4.2. Classification of constitutive and hydrodynamic instabilities

It is well-known in continuum mechanics that the nonlinearities in constitutive laws can lead to certain instabilities, commonly known as *constitutive/material* instability (Hadamard 1903; Joseph & Saut 1986; see, for a review, Goddard & Alam 1999). The non-monotonic stress–strain curve or the coil–stretch transition (de Gennes 1974) in polymer rheology are classic examples of such instabilities. At the onset of constitutive instability, the underlying field equations undergo a change of type (Joseph & Saut 1986) in the form of either a loss of hyperbolicity, or a loss of ellipticity. These instabilities differ from their well-known hydrodynamic counterpart in that the nonlinearities associated with inertial terms are primarily responsible for the latter type of instability. Following Goddard & Alam (1999), we classify the streamwise-independent instabilities of granular shear flow in terms of constitutive instability.

The criterion for the onset of the pure transverse instability is $\mathcal{N}_2(v, e) > 0$ (refer to (3.2)), which can be translated into

$$\frac{d}{dv} \left(\frac{\sqrt{f_2 f_5}}{f_1} \right) > 0. \quad (4.4)$$

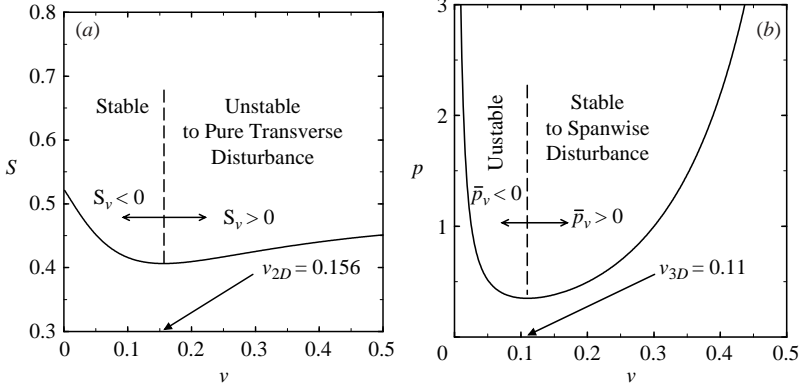


FIGURE 16. Variations of (a) the shear-to-pressure ratio, $S = \mu/p$, and (b) the pressure, p , with solid fraction for uniform-shear flow. The regions of (in)stability to pure transverse and spanwise perturbations are demarcated by the dashed line in each panel.

The term within the brackets is the ratio between the shear stress and the pressure, $S = \mu/p$, whose variation with density is clearly non-monotonic as shown in figure 16(a). And the flow is unstable beyond a minimum solid fraction at which S_v changes sign:

$$v_{2D} \equiv v|_{S_v=0}.$$

Thus, the origin of the transverse-banding instability is tied to the non-monotonicity of the shear-to-normal stress ratio with density. This instability criterion (4.4) is similar to the criterion for the ordering transition in a sheared dense molecular fluid (Loose & Hess 1989) as discussed in Appendix B.

Similarly, the criterion for the onset of the pure spanwise instability (refer to (3.9)) can be rearranged to yield

$$\frac{d}{dv} \left(\frac{f_1 f_2}{f_5} \right) < 0. \quad (4.5)$$

Note that the term within the brackets is the pressure for the uniform-shear flow, $p = f_1 f_2 / f_5$, which also varies non-monotonically with density as shown in figure 16(b). Hence, the flow is unstable to pure spanwise perturbations below a critical solid fraction where p_v changes sign:

$$v_{3D} \equiv v|_{p_v=0}.$$

Thus, the origin of the spanwise-banding instability in uniform shear flow is tied to the non-monotonicity of pressure with density.

This brings us to an important issue: do the streamwise granular structures belong to the same class as that of the well-known Taylor–Couette vortices of Newtonian fluids? The answer is negative since the Taylor–Couette vortices are hydrodynamic in origin and the granular vortices are constitutive in origin. Thus, despite having certain structural similarities, the streamwise granular vortices that we have predicted are distinctly different from their Newtonian counterparts in Taylor–Couette flows.

4.2.1. Spanwise banding and the loss of hyperbolicity

Here I show that the pure spanwise instability of granular shear flow can be predicted by considering the stability of a reduced model of an isothermal sheared granular fluid, which also suggests a change of type of an underlying wave equation at the instability onset.

Let us assume that *the role of granular energy equation is only to set the temperature of the base state, and that the predicted instabilities are independent of this equation.* Thus, the granular fluid is isothermal with the granular temperature: $T(v, e) = f_2/f_5$. Since the granular energy equation is redundant for this ‘reduced’ model, we have to deal only with the continuity and momentum equations with the following ‘effective’ transport coefficients:

$$\left. \begin{aligned} \mu &\equiv \mu(v, e) = f_2^{3/2}/f_5^{1/2}, \\ p &\equiv p(v, e) = f_1 f_2/f_5, \\ \lambda &\equiv \lambda(v, e) = (f_3 - \frac{2}{3}f_2)(f_2/f_5)^{1/2}. \end{aligned} \right\} \quad (4.6)$$

For this model with pure spanwise perturbations, the streamwise and transverse shear modes decay in the asymptotic limit (as in the full model, see equation (3.5)). The spanwise shear mode can be shown to satisfy the following partial differential equation:

$$\frac{\partial^2 w'}{\partial t^2} = p_v H^{-2} \frac{\partial^2 w'}{\partial z^2} + \left(\frac{2\mu + \lambda}{v H^2} \right) \frac{\partial^3 w'}{\partial z^2 \partial t}. \quad (4.7)$$

Using the standard normal-mode decomposition ($w'(z, t) \sim e^{\omega t} e^{ik_z z}$), the dispersion relation reduces to

$$\omega^2 + \left(\frac{2\mu + \lambda}{v H^2} \right) k_z^2 \omega + p_v H^{-2} k_z^2 = 0. \quad (4.8)$$

The two roots of this equation are given by

$$\omega_{1,2} = \frac{1}{2} \left(\frac{2\mu + \lambda}{v H^2} \right) k_z^2 \left[-1 \pm \sqrt{1 - p_v \left(\frac{2vH}{(2\mu + \lambda)k_z} \right)^2} \right]. \quad (4.9)$$

It is clear that the negativity of p_v leads to a stationary instability, with $p_v = 0$ indicating the onset of instability. The growth rate of this instability increases with increasing k_z and becomes unbounded as $k_z \rightarrow \infty$. Hence this is a short-wave instability of Hadamard type (Hadamard 1903). When we include the granular-energy equation, these short waves are damped, beyond a finite cutoff value of k_z , by the conduction term (see the expression for \mathcal{N}_1 in equation (3.2)). It can be verified that the evolution equation for density perturbations reduces to the following equation (neglecting the source terms due to viscosity):

$$\frac{\partial^2 v'}{\partial t^2} = D \frac{\partial^2 v'}{\partial z^2}, \quad \text{with } D = p_v. \quad (4.10)$$

This is the well-known wave equation, and is of hyperbolic type when D is positive for which the flow remains stable. For instability to occur we must have a negative D , rendering the above equation of elliptic type. Hence, the onset of the pure spanwise instability is tied to the loss of hyperbolicity of the above wave equation.

It is important to note that there is no change in type of the field equations when we consider the full set of equations. Only for the ‘reduced-model’ (with isothermal approximation) have we derived the wave equation for density perturbation for the pure spanwise modes which loses hyperbolicity at the onset of instability. As mentioned before, this instability survives only at long wavelengths ($k \sim 0$) since the short waves are regularized by the conduction term in the granular-energy equation.

4.3. Choice of constitutive model and the effects of inelasticity

The present work is based on the Newtonian constitutive model of Lun *et al.* (1984) since we wanted make a direct comparison with a previous work on stability (Alam & Nott 1998). The Newtonian constitutive model can be obtained from the Enskog–Boltzmann equation by employing the perturbative expansion procedure of Chapman and Enskog, and then truncating the infinite series at the Navier–Stokes order. By including the Burnett- and super Burnett-order terms, one can obtain a non-Newtonian constitutive model (Sela & Goldhirsch 1998; Jin & Slemrod 2001; Santos, Garzo & Dufty 2004).

The Newtonian constitutive model is strictly valid for nearly elastic systems ($e \rightarrow 1$). However, the qualitative nature of our results would not change even if we were to use any other Newtonian model. For example, we have shown that the streamwise-independent ‘constitutive’ instabilities are quite robust and depend only on the variation of pressure and viscosity with density (see figure 16). We have checked that the shape of these curves does not change whether we use the model of Lun *et al.* (1984) or Jenkins & Richman (1985); only the critical solid fractions (ν_{2D} and ν_{3D}) for the onset of such instabilities differ slightly. It is straightforward to verify that the inclusion of an additional contribution to the collisional dissipation \mathcal{D} , that is proportional to $\nabla \cdot \mathbf{u}$ (Garzo & Dufty 1999), does not influence the above conclusion. In this regard, we also need to mention that both ν_{2D} and ν_{3D} increase slightly if we use the Carnahan and Starling form of the radial distribution function.

The choice of $e = 0.8$ in most of the figures is based on an earlier work (Alam & Nott 1998). We have checked that all the instabilities survive for any value of $e \neq 1$. As we approach the elastic limit ($e \rightarrow 1$), the growth rate of any instability (except the dilute flow instabilities in figure 12) decreases and the critical Couette gap (H) for the onset of instability increases. Of course, for highly dissipative systems, one should use non-Newtonian constitutive models that incorporate normal stress differences (Alam & Luding 2003). It is possible that such higher-order corrections might introduce new instabilities (see, for example, Kumaran 2004). Our preliminary work based on a relaxation-type non-Newtonian model suggests that there are new travelling wave instabilities at moderate densities if the relaxation time is of order one or larger; the details of these results will be published in the future.

5. Summary and conclusions

We have investigated the stability of the bounded uniform shear flow of granular materials to three-dimensional perturbations, using a kinetic-theory-based Newtonian constitutive model for the rheology of the granular medium. This flow is found to be unstable to pure spanwise ($k_z \neq 0$, but $k_x = 0$ and $\partial/\partial y(\cdot) = 0$, where k_i is the wavenumber for the i th direction) stationary perturbations if the solid fraction is below some critical value $\nu < \nu_{3D}$ (~ 0.1), leading to the banding of particles along the spanwise direction. However, beyond a moderate value of the solid fraction $\nu > \nu_{2D}$ (~ 0.15), the most unstable streamwise-independent ($k_x = 0$) mode is a two-dimensional stationary perturbation, leading to the banding of particles along the transverse direction (i.e. a pure transverse mode). The growth rates of the pure spanwise instabilities are an order-of-magnitude larger than of the pure transverse instabilities. Both these spanwise and transverse instabilities lead to structures having no variation in the streamwise direction, and they are responsible for the generation of the streamwise structures. Similar types of vortices have recently been observed in

three-dimensional molecular dynamics simulations of dilute granular Couette flows (Conway & Glasser 2004).

For non-zero values of the streamwise wavenumber ($k_x \neq 0$), additional three-dimensional instabilities in the form of both travelling and stationary waves appear at moderate-to-large mean densities ($\nu > \nu_{3D}$). The origin of these three-dimensional instabilities is traced back to the corresponding two-dimensional instabilities. The growth rates of both the travelling and stationary instabilities decrease with increasing spanwise wavenumber, and hence the dominant instability still comes from two-dimensional perturbations. Interestingly, the inclusion of spanwise perturbations changes the density patterns in the shear plane in that a row of clusters for two-dimensional perturbations splits into two rows of clusters for three-dimensional perturbations. For very long streamwise modes ($k_x \sim 0$), we find the birth of travelling vortices which are simply the modulated versions of the corresponding pure streamwise vortices.

In the dilute regime ($\nu < \nu_{3D}$), the dominant instability comes from the pure spanwise ('stationary') modes but there are three-dimensional 'travelling' instabilities of comparable growth rates with $k_x = O(1)$. The origin of these 'new' travelling instabilities is tied to the corresponding pure spanwise instabilities. These travelling waves are associated with large-scale vortical motions near the walls. The nonlinear saturation of these instabilities will lead to 'asymmetric' travelling density patterns, with the asymmetry being in the transverse direction.

The effects of boundary conditions on three-dimensional instabilities are similar to those on their two-dimensional counterparts, as long as the base flow remains similar to that of the uniform-shear flow. For some dilute-flow instabilities (that lead to vertical columnar-type density patterns), we have found that they can disappear with the inclusion of the wall slip.

We have classified the streamwise-independent instabilities (leading to transverse and spanwise bandings) in terms of 'constitutive' instability (Hadamard 1903; de Gennes 1974; Joseph & Saut 1986; Goddard & Alam 1999). While the non-monotonicity of the pressure with density signals the onset of the pure spanwise instability, the non-monotonicity of the shear-to-normal stress ratio with density signals the onset of the pure transverse instability. Using a reduced model of an isothermal granular fluid, we have shown that both these instabilities are short waves in nature, and are regularized by the conduction term in the granular-energy equation. We have further shown that the onset of pure spanwise instability can be tied to the loss of hyperbolicity of an underlying wave equation. We conclude that the streamwise granular vortices are distinctly different from the stationary Taylor–Couette vortices of Newtonian fluids, since the former is a constitutive instability and the latter a hydrodynamic instability.

As mentioned briefly in the introductory section, there are numerous works that unveil the route to turbulence in Newtonian fluids, and the streamwise vortices play an important role in such a transition scenario (Schmid & Henningson 2001). Since turbulence is an inertial phenomenon, the pure streamwise vortices that originate from constitutive instabilities would not lead to turbulence. However, we have also uncovered modulated streamwise vortices that are hydrodynamic in origin, and they might lead to turbulence-like activity in granular fluids. To establish a firm connection of the present work to granular turbulence, we need to solve the nonlinear hydrodynamic equations, starting with such streamwise vortices as initial conditions. Another possibility is to choose appropriate initial conditions from the 'non-modal' transient stability analysis of granular flows which also yields streamwise vortices as

the optimal perturbations (Gayen & Alam 2005). Some recent MD simulations have probed the possibility of turbulence in freely cooling granular media via the vortex route (Isobe 2003). Clearly, similar MD simulations on granular shear flow would further test the proposed route to turbulence.

The effects of streamwise vortices on the plugged base states with wall-slip and non-zero heat-flux boundary conditions remain unexplored. It would be interesting to further investigate the stability of such plugged base states to three-dimensional perturbations, complemented by MD simulations at moderate-to-large densities. Lastly, it would be desirable to analyse the effects of non-Newtonian rheology (i.e. the normal stress differences) on the predicted instabilities, which, however, requires a Burnett-order constitutive model. Work in these directions is in progress.

I acknowledge financial support from JNCASR in the form of a start-up grant (PC/EMU/MA/35).

Appendix A. Governing equations and boundary conditions

Using the wall-to-wall gap \tilde{H} as the length scale, the velocity difference between the walls \tilde{u}_w as the velocity scale and the inverse of the overall shear rate $\tilde{H}/\tilde{u}_w \equiv \tilde{\gamma}^{-1}$ as the time scale, the dimensionless evolution equations for $v(x, y, z, t)$, $u(x, y, z, t)$, $w(x, y, z, t)$ and $T(x, y, z, t)$ can be written as

$$\frac{Dv}{Dt} = -v\nabla \cdot \mathbf{u}, \quad (\text{A } 1)$$

$$\begin{aligned} v \frac{Du}{Dt} = & -\frac{1}{H^2} \frac{\partial p}{\partial x} + \frac{1}{H^2} \frac{\partial}{\partial x} \left[2\mu \frac{\partial u}{\partial x} + \lambda(\nabla \cdot \mathbf{u}) \right] \\ & + \frac{1}{H^2} \frac{\partial}{\partial y} \left[\mu \left(\frac{\partial u}{\partial y} + \frac{\partial v}{\partial x} \right) \right] + \frac{1}{H^2} \frac{\partial}{\partial z} \left[\mu \left(\frac{\partial u}{\partial z} + \frac{\partial w}{\partial x} \right) \right], \end{aligned} \quad (\text{A } 2)$$

$$\begin{aligned} v \frac{Dv}{Dt} = & -\frac{1}{H^2} \frac{\partial p}{\partial y} + \frac{1}{H^2} \frac{\partial}{\partial y} \left[2\mu \frac{\partial v}{\partial y} + \lambda(\nabla \cdot \mathbf{u}) \right] \\ & + \frac{1}{H^2} \frac{\partial}{\partial z} \left[\mu \left(\frac{\partial v}{\partial z} + \frac{\partial w}{\partial y} \right) \right] + \frac{1}{H^2} \frac{\partial}{\partial x} \left[\mu \left(\frac{\partial u}{\partial y} + \frac{\partial v}{\partial x} \right) \right], \end{aligned} \quad (\text{A } 3)$$

$$\begin{aligned} v \frac{Dw}{Dt} = & -\frac{1}{H^2} \frac{\partial p}{\partial z} + \frac{1}{H^2} \frac{\partial}{\partial z} \left[2\mu \frac{\partial w}{\partial z} + \lambda(\nabla \cdot \mathbf{u}) \right] \\ & + \frac{1}{H^2} \frac{\partial}{\partial x} \left[\mu \left(\frac{\partial u}{\partial z} + \frac{\partial w}{\partial x} \right) \right] + \frac{1}{H^2} \frac{\partial}{\partial y} \left[\mu \left(\frac{\partial v}{\partial z} + \frac{\partial w}{\partial y} \right) \right], \end{aligned} \quad (\text{A } 4)$$

$$\begin{aligned} \frac{3}{2}v \frac{DT}{Dt} = & \frac{1}{H^2} \nabla \cdot (\kappa \nabla T + \kappa_h \nabla v) - p(\nabla \cdot \mathbf{u}) \\ & + 2\mu \left[\left(\frac{\partial u}{\partial x} \right)^2 + \left(\frac{\partial v}{\partial y} \right)^2 + \left(\frac{\partial w}{\partial z} \right)^2 + \frac{1}{2} \left(\frac{\partial u}{\partial y} + \frac{\partial v}{\partial x} \right)^2 \right. \\ & \left. + \frac{1}{2} \left(\frac{\partial v}{\partial z} + \frac{\partial w}{\partial y} \right)^2 + \frac{1}{2} \left(\frac{\partial w}{\partial x} + \frac{\partial u}{\partial z} \right)^2 + \frac{\lambda}{2\mu} (\nabla \cdot \mathbf{u})^2 \right] - \mathcal{D}, \end{aligned} \quad (\text{A } 5)$$

where $D/Dt = \partial/\partial t + \mathbf{u} \cdot \nabla$ is the material derivative, \mathcal{D} the collisional dissipation rate per unit volume (in dimensionless form) and $H = \tilde{H}/\tilde{d}$ the dimensionless wall separation or the Couette gap. The dimensionless transport coefficients take the

following form:

$$\left. \begin{aligned} p(\nu, T) &= f_1(\nu, e) T, & \mu(\nu, T) &= f_2(\nu, e) T^{1/2}, \\ \zeta(\nu, T) &= f_3(\nu, e) T^{1/2}, & \lambda(\nu, T) &= \left(\zeta - \frac{2}{3}\mu\right), \\ \kappa(\nu, T) &= f_4(\nu, e) T^{1/2}, & \kappa_h(\nu, T) &= f_{4h}(\nu, e) T^{3/2}, \\ \mathcal{D}(\nu, T) &= f_5(\nu, e) T^{3/2}. \end{aligned} \right\} \quad (\text{A } 6)$$

Here $f_1 - f_5$ are the non-dimensional functions of ν and e (see table 1 of Alam & Nott 1998).

We adopt the boundary conditions of Johnson & Jackson (1987). The boundary conditions on velocity and granular temperature, in dimensionless form, can be written as

$$\frac{\mathbf{u}_s}{|\mathbf{u}_s|} \cdot \boldsymbol{\Sigma} \cdot \mathbf{n} = H \frac{\mathbf{u}_s}{|\mathbf{u}_s|} \cdot \mathbf{S}^w, \quad (\text{A } 7)$$

$$\mathbf{n} \cdot \mathbf{q} = H^3 \mathbf{u}_s \cdot \mathbf{S}^w - H \mathcal{D}^w, \quad (\text{A } 8)$$

respectively. Here $\boldsymbol{\Sigma}$ is the ‘fluid’ stress tensor, \mathbf{S}^w is the tangential momentum flux at the wall, \mathbf{q} is the heat flux vector, \mathcal{D}^w the dissipation rate (due to inelastic grain–wall collisions) per unit volume, \mathbf{n} the unit normal from the wall directed into the particle assembly, and $\mathbf{u}_s = \mathbf{u} - \mathbf{u}_w$ the wall slip, with \mathbf{u} being the velocity of the granular material in contact with the wall and \mathbf{u}_w the wall velocity. The expressions for \mathbf{S}^w and \mathcal{D}^w are (Johnson & Jackson 1987)

$$\mathbf{S}^w = \frac{\phi \sqrt{3} \pi \nu \chi T^{1/2} \mathbf{u}_s}{6\nu_{max}} \quad \text{and} \quad \mathcal{D}^w = \frac{\sqrt{3} \pi \nu \chi T^{3/2} (1 - e_w^2)}{4\nu_{max}}. \quad (\text{A } 9)$$

The specularity coefficient (or the momentum accommodation coefficient), ϕ , characterizes the overall roughness of the wall, and its value varies between zero (for perfectly specular collisions with a smooth wall) and unity (for perfectly diffuse collisions with a rough wall); e_w is the coefficient of restitution for particle–wall collisions.

Appendix B. Connection with the stability criterion of Loose & Hess

There is an interesting connection of our instability criterion (4.4) for transverse banding with a similar ordering transition in dense molecular fluids (Loose & Hess 1989). The instability criterion for the ordering transition of Loose & Hess is given by

$$\left(\frac{\partial p_{yx}}{\partial \gamma}\right) \left(\frac{\partial p_{yy}}{\partial \rho}\right) \leq \left(\frac{\partial p_{yx}}{\partial \rho}\right) \left(\frac{\partial p_{yy}}{\partial \gamma}\right), \quad (\text{B } 1)$$

where ρ is the density, γ the shear rate, p_{yx} is the shear stress and p_{yy} is the isotropic pressure in the present context. We assume the following functional dependence for the normal and shear stresses on density and shear rate,

$$\left. \begin{aligned} p_{yy} &= p_{yy}(\rho) f_{yy}(\gamma), \\ p_{yx} &= p_{yx}(\rho) f_{yx}(\gamma), \end{aligned} \right\} \quad (\text{B } 2)$$

where $f_{yy}(\gamma)$ and $f_{yx}(\gamma)$ represent nonlinear functions of shear rate. Therefore, the instability criterion (B 1) can be rewritten as

$$\left(p_{yx} \frac{df_{yx}}{d\gamma}\right) \left(f_{yy} \frac{dp_{yy}}{d\rho}\right) \leq \left(f_{yx} \frac{dp_{yx}}{d\rho}\right) \left(p_{yy} \frac{df_{yy}}{d\gamma}\right). \quad (\text{B } 3)$$

For a granular fluid, the dependences of stresses on the shear rate and granular temperature are given by

$$\left. \begin{aligned} f_{yy}(\gamma) &\sim T, \\ f_{yx}(\gamma) &\sim \gamma\sqrt{T}. \end{aligned} \right\} \quad (\text{B 4})$$

From the energy-balance equation of steady uniform-shear flow, we have the following expression for the granular temperature:

$$T = \left(\frac{f_2}{f_5}\right)\gamma^2 \sim \gamma^2. \quad (\text{B 5})$$

Hence, the shear-rate dependence of stresses for a granular fluid is given by

$$\left. \begin{aligned} f_{yy}(\gamma) &= \gamma^2, \\ f_{yx}(\gamma) &= \gamma^2, \end{aligned} \right\} \quad (\text{B 6})$$

i.e. the stresses vary quadratically with the shear rate (representing the well-known Bagnold-scaling) and the viscosity varies linearly with the shear rate. Thus, the granular fluid is non-Newtonian which is, however, a consequence of the higher-order balance equation for the granular temperature. With these scalings, the instability criterion (B 1) of Loose & Hess reduces to

$$\begin{aligned} p_{yx} \frac{dp_{yy}}{d\rho} &\leq p_{yy} \frac{dp_{yx}}{d\rho} \\ \Rightarrow \frac{d}{d\rho} \left[\frac{p_{yx}}{p_{yy}} \right] &\geq 0. \end{aligned} \quad (\text{B 7})$$

This is nothing but our instability criterion (4.4) for the transverse banding in granular shear flow.

REFERENCES

- ALAM, M. 2005 Universal unfolding of pitchfork bifurcations and the shear-band formation in rapid granular Couette flow. In *Trends in Applications of Mathematics to Mechanics* (ed. Y. Wang & K. Hutter), pp. 11–20. Shaker-Verlag, Aachen.
- ALAM, M., ARAKERI, V. H., NOTT, P. R., GODDARD, J. & HERRMANN, H. J. 2005 Instability-induced ordering, universal unfolding and the role of gravity in granular Couette flow. *J. Fluid Mech.* **523**, 277.
- ALAM, M. & LUDING, S. 2003 First normal stress difference and crystallization in a dense sheared granular fluid. *Phys. Fluids* **15**, 2298.
- ALAM, M. & NOTT, P. R. 1997 The influence of friction on the stability of unbounded granular Couette flow. *J. Fluid Mech.* **343**, 267.
- ALAM, M. & NOTT, P. R. 1998 Stability of plane Couette flow of a granular material. *J. Fluid Mech.* **377**, 99.
- BABIĆ, M. 1993 On the stability of rapid granular flows. *J. Fluid Mech.* **254**, 127.
- CARPEN, I. C. & BRADY, J. F. 2002 Gravitational instability in suspension flow. *J. Fluid Mech.* **472**, 201.
- COLE, D. 1965 Transition in circular Couette flow. *J. Fluid Mech.* **21**, 385.
- CONWAY, S. L. & GLASSER, B. J. 2004 Density waves and coherent structures in granular Couette flow. *Phys. Fluids* **16**, 509.
- FISCHER, F., WHEELER, E. & FULLER, G. G. 2002 Shear-banding structure oriented in the vorticity direction observed for equimolar micellar solution. *Rheol. Acta* **41**, 35.
- FORNBERG, B. 1998 *A Practical Guide to Pseudospectral Methods*. Cambridge University Press.
- FORTERRE, F. & POULIQUEN, O. 2002 Stability analysis of rapid granular chute flows: formation of longitudinal vortices. *J. Fluid Mech.* **467**, 361.

- GARZO, V. & DUFTY, J. 1999 Dense fluid transport for inelastic hard spheres. *Phys. Rev. E* **59**, 5895.
- GAYEN, B. & ALAM, M. 2005 Algebraic and exponential instabilities in a sheared micropolar granular fluid. *J. Fluid Mech.* (submitted).
- DE GENNES, P. G. 1974 Coil-stretch transition of dilute flexible polymers under ultra-high gradients. *J. Chem. Phys.* **60**, 5030.
- GODDARD, J. & ALAM, M. 1999 Shear-flow and material instabilities in particulate suspensions and dry granular media. *Particulate Sci. Technol.* **17**, 69.
- GOLDFARB, D. J., GLASSER, B. J. & SHINBROT, T. 2002 Shear instabilities in granular flows. *Nature* **415**, 302.
- GOLDHIRSCH, I. 2003 Rapid granular flows. *Annu. Rev. Fluid Mech.* **35**, 267.
- GOLDHIRSCH, I. & ZANETTI, D. 1993 Clustering instability in dissipative gases. *Phys. Rev. Lett.* **70**, 1619.
- HADAMARD, J. 1903 *Lecons sur la Propagation des Ondes et les Équations de l'Hydrodynamique*. Paris. (Chelsea Publishing Company: New York. Reprinted in 1949.)
- HAMILTON, J. M. & ABERNATHY, F. H. 1994 Streamwise vortices and transition to turbulence. *J. Fluid Mech.* **264**, 185.
- HOPKINS, M. A., JENKINS, J. T. & LOUGE, M. Y. 1993 On the structure of three-dimensional shear flows. In *Advances in Micromechanics of Granular Materials* (ed. H. H. Shen, M. Satake, M. Mehrabadi, C. S. Chang & C. S. Campbell), pp. 271–279. Elsevier.
- ISOBE, M. 2003 Velocity statistics in two-dimensional granular turbulence. *Phys. Rev. E* **68**, 040301-1.
- JENKINS, J. T. & RICHMAN, M. W. 1985 Grad's 13-moment system for a dense gas of inelastic spheres. *Arch. Rat. Mech. Anal.* **87**, 355.
- JIN, S. & SLEMROD, M. 2001 Regularization of the Burnett equations for rapid granular flows via relaxation. *Physica D* **150**, 207.
- JOHNSON, P. C. & JACKSON, R. 1987 Frictional-collisional constitutive relations for granular materials, with application to plane shearing. *J. Fluid Mech.* **176**, 67.
- JOSEPH, D. D. & SAUT, J. C. 1986 Change of type and loss of evolution in the flow of viscoelastic fluids. *J. Non-Newtonian Fluid Mech.* **20**, 117.
- KADANOFF, L. 1999 Built upon sand: Theoretical ideas inspired by granular flows. *Rev. Mod. Phys.* **64**, 111.
- KUMARAN, V. 2004 Constitutive relations and linear stability of a sheared granular flow. *J. Fluid Mech.* **506**, 1.
- LOOSE, W. & HESS, S. 1989 Rheology of dense model fluids via nonequilibrium molecular dynamics: shear-thinning and ordering transition. *Rheol. Acta* **28**, 101.
- LUDING, S. & HERRMANN, H. J. 1999 Clustering in granular gases. *Chaos* **9**, 673.
- LUN, C. K. K., SAVAGE, S. B., JEFFREY, D. J. & CHEPURNIY, N. 1984 Kinetic theories for granular flow: inelastic particles in Couette flow and slightly inelastic particles in a general flow field. *J. Fluid Mech.* **140**, 223.
- MCMANARA, S. 1993 Hydrodynamic modes of a uniform granular medium. *Phys. Fluids A* **5**, 3056.
- MELLO, T. M., DIAMOND, P. H. & LEVINE, H. 1991 Hydrodynamic modes of granular shear flow. *Phys. Fluids A* **3**, 2067.
- NOTT, P. R., ALAM, M., AGRAWAL, K., JACKSON, R. & SUNDARESAN, S. 1999 The effect of boundaries on the plane Couette flow of granular materials: a bifurcation analysis. *J. Fluid Mech.* **397**, 234.
- OTTINO, J. M. & KHAKHAR, D. V. 2000 Segregation and mixing in granular flows. *Annu. Rev. Fluid Mech.* **32**, 55.
- POULIQUEN, O., DELOUR, J. & SAVAGE, S. B. 1997 Fingering in granular flows. *Nature* **386**, 816.
- SANTOS, A., GARZO, V. & DUFTY, J. 2004 Inherent rheology of a granular fluid in uniform shear flow. *Phys. Rev. E* **69**, 061303-1.
- SAVAGE, S. B. 1992 Instability of unbounded uniform granular shear flow. *J. Fluid Mech.* **241**, 109.
- SCHMID, P. J. & HENNINGSON, D. S. 2001 *Stability and Transition in Shear Flows*. Springer.
- SCHMID, P. J. & KYTÖMAA, H. K. 1994 Transient and asymptotic stability of granular shear flow. *J. Fluid Mech.* **264**, 255.
- SELA, N. & GOLDHIRSCH, I. 1998 Hydrodynamic equations for rapid shear flows of smooth, inelastic spheres, to Burnett order. *J. Fluid Mech.* **361**, 41.

- TAN, M.-L. 1995 Microstructure and macrostructures in rapid granular flows. PhD thesis, Princeton University, USA.
- TAN, M.-L. & GOLDBIRSCHE, I. 1997 Intercluster interactions in rapid granular shear flows. *Phys. Fluids* **9**, 856.
- WALEFFE, F. 2003 Homotopy of exact structures in plane shear flows. *Phys. Fluids* **15**, 1517.
- UMBANHOWER, P., MELO, F. & SWINNEY, H. L. 1996 Oscillons in vibrated granular media. *Nature* **382**, 793.
- WANG, C., JACKSON, R. & SUNDARESAN, S. 1996 Stability of bounded rapid shear flows of a granular material. *J. Fluid Mech.* **308**, 31.